

FINNISH METEOROLOGICAL INSTITUTE  
CONTRIBUTIONS

No. 42

GEOMAGNETIC INDUCTION DURING HIGHLY DISTURBED  
SPACE WEATHER CONDITIONS: STUDIES OF GROUND  
EFFECTS

Antti Pulkkinen

Department of Physical Sciences  
Faculty of Science  
University of Helsinki  
Helsinki, Finland

ACADEMIC DISSERTATION in physics

To be presented, with the permission of the Faculty of Science of the University of Helsinki, for public criticism in Small Auditorium E204 at Physicum in Kumpula Campus on August 30th, 2003, at 10 a.m.

Finnish Meteorological Institute  
Helsinki, 2003

ISBN 951-697-579-8 (paperback)

ISBN 952-10-1253-6 (pdf)

ISSN 0782-6117

Yliopistopaino

Helsinki, 2003



FINNISH METEOROLOGICAL INSTITUTE

Published by Finnish Meteorological Institute  
P.O. Box 503  
FIN-00101 Helsinki, Finland

Series title, number and report code of publication  
Contributions 42, FMI-CONT-42

Date June 2003

Authors  
Antti Pulkkinen

Name of project

Commissioned by

Title

Geomagnetic induction during highly disturbed space weather conditions: Studies of ground effects

Abstract

The thesis work tackles the end of the space weather chain. By means of both theoretical and data-based investigations the thesis provides new tools and physical understanding of the processes related to geomagnetic induction and its effects on technological systems on the ground during highly disturbed geomagnetic conditions. In other words, the thesis focuses on geomagnetically induced currents (GIC). Noteworthy is also that GIC research is a practical interface between the solid Earth and space physics domains.

It is shown that GIC can be modeled accurately with rather simple mathematical tools requiring that the topology and the electrical parameters of the conductor system, the ground conductivity structure and either the ionospheric source current or the ground magnetic field variations are known. Data-based investigations revealed that from the geophysical viewpoint, the character of GIC events is twofold. On one hand, large GIC can be observed at the same time instant throughout the entire auroral region. On the other hand, spatial and temporal scales related to these events are rather small making the detailed behavior of individual GIC events relatively local. It was observed that although substorms are statistically the most important drivers of large GIC in the auroral region, there are a number of different magnetospheric mechanisms capable to such dynamic changes that produce large GIC.

Publishing unit

Geophysical Research

Classification (UDC)  
52-85, 550.38

Keywords

Geomagnetically induced currents, geomagnetic disturbances, space weather

ISSN and series title

0782-6117 Finnish Meteorological Institute Contributions

ISBN

951-697-579-8(paperback), 952-10-1253-6(pdf)

Language

English

Sold by

Finnish Meteorological Institute / Library  
P.O.Box 503, FIN-00101 Helsinki  
Finland

Pages 164

Price

Note



Väitöstyö käsittelee avaruussäätöjen loppupäätä, geomagneettisten häiriöiden vaikutuksia maanpinnan teknologisiin johdinjärjestelmiin. Toisin sanoen työssä tarkastellaan geomagneettisesti indusoituneita virtoja (GIC). Työ tuo teoreettisten ja havaintoihin perustuvien tarkastelujen avulla sekä uusia työkaluja että uutta fysikaalista ymmärrystä avaruussäätöjen maanpintavaikutuksiin. Työ osoittaa konkreettisesti kuinka GIC-tutkimus on rajapinta avaruusfysiikan ja maaperän tutkimuksen välillä.

Väitöstyö osoittaa, että GIC:tä voidaan mallintaa tarkasti varsin yksinkertaisten matemaattisten menetelmien avulla. Mallinnus edellyttää, että johdinjärjestelmän topologia ja sähköiset ominaisuudet, maan johtavuusrakenne ja ionosfäärin virtojen tai maanpinnan magneettikentän käyttäytyminen tunnetaan. Havaintoihin perustuvat tarkastelut paljastivat, että GIC-ilmiö on geofysikaalisilta ominaisuuksiltaan kaksijakoinen. Toisaalta suuria induktiovirtoja voidaan havaita samaan aikaan kaikkialla revontulialueella. Toisaalta taas ilmiöön liittyvät aika- ja paikkaskaalat ovat verrattain pieniä, joten GIC:n yksityiskohtainen käyttäytyminen on hyvin paikallista. Havaittiin, että vaikkakin geomagneettiset alimyrskyt ovat tilastollisesti kaikkein merkittävin suurien GIC:den aiheuttaja, myös lukuisat muut magnetosfäärin dynaamiset muutokset voivat aiheuttaa merkittäviä vaikutuksia maanpinnan teknologisissa johdinjärjestelmissä.

# Preface

In the wake of the emerging science of space weather, the effects of our near space environment on technological systems both on the ground and in space have received growing attention through the late 1990's and beginning of the new millennium. Because of the apparent attractiveness of the subject, large number of recent scientific work has fallen, or been dropped, under the realm of space weather and even commercial companies have been established to serve the interests of the industry. However, despite the existing commercial activities, the size of the market for such a service is not yet well known and is under a constant debate. In addition, there is still no definite picture about the true nature of the risk that space weather related phenomena pose on different systems. The presently ongoing Space Weather Pilot Projects funded by the European Space Agency, will hopefully enlighten the size of the space weather market and give some quantitative measures for the impact of space weather on technological systems in the near future.

Regardless of the economical importance, space weather can be thought of as an ultimate test of our scientific understanding about our near space and its coupling to the Earth surface environment, and is by far the most important motivation for the thesis at hand. In order to be able to model, and eventually, forecast, the Earth surface effects due to some specific event on the Sun, we have to be able to describe in quite good detail the physical behavior of the entire Sun - solar wind - magnetosphere - ionosphere - ground chain. The chain is governed by processes which require a number of different physical approaches, and it is clear that convergence of multi-disciplinary science is needed before a consistent picture of the phenomena can emerge. Space weather is an umbrella unifying different branches of science for establishing a collective picture of our constantly broadening environment.

The thesis presented addresses the end link of the space weather chain. By means of both theoretical and data-based investigations the thesis attempts to provide new tools and physical understanding of the processes

related to geomagnetic induction and its effects on technological systems on the ground during highly disturbed geomagnetic conditions. In other words, the thesis focuses on *geomagnetically induced currents* (GIC), to use the general term given for the phenomena.

The work done in the thesis is presented in five papers published in international journals. The papers are the following:

**I)** Pulkkinen, A., R. Pirjola, D. Boteler, A. Viljanen, and I. Yegorov, Modelling of space weather effects on pipelines, *Journal of Applied Geophysics*, **48**, 233, 2001a.

**II)** Pulkkinen, A., A. Viljanen, K. Pajunpää, and R. Pirjola, Recordings and occurrence of geomagnetically induced currents in the Finnish natural gas pipeline network, *Journal of Applied Geophysics*, **48**, 219, 2001b.

**III)** Pulkkinen, A., O. Amm, A. Viljanen, and BEAR Working Group, Ionospheric equivalent current distributions determined with the method of spherical elementary current systems, *Journal of Geophysical Research*, **108**, doi: 10.1029/2001JA005085, 2003a.

**IV)** Pulkkinen, A., A. Thomson, E. Clarke, and A. McKay, April 2000 geomagnetic storm: ionospheric drivers of large geomagnetically induced currents, *Annales Geophysicae*, **21**, 709, 2003b.

**V)** Pulkkinen, A., O. Amm, A. Viljanen, and BEAR Working Group, Separation of the geomagnetic variation field on the ground into external and internal parts using the spherical elementary current system method, *Earth, Planets and Space*, **55**, 117, 2003c.

Summarizing, the work made in these papers is:

**I)** An extension of the distributed source transmission line (DSTL) theory (Boteler and Cookson, 1986) was introduced to the computation of the induced currents and pipe-to-soil voltages in complex pipeline networks. The method was tested by three-dimensional simulations and by comparing measured and modeled GIC.

**II)** The method developed in Paper I was applied to the Finnish natural gas pipeline. Using measurements of GIC in the pipeline, carried out by the Finnish Meteorological Institute, and recordings of the geomagnetic

field at the Nurmijärvi Geophysical Observatory, statistical occurrence for GIC and pipe-to-soil voltages at different parts of the Finnish pipeline were derived.

**III)** A novel Spherical Elementary Currents System (SECS) method developed by Amm (1997) and Amm and Viljanen (1999) for the determination of ionospheric equivalent currents was rigorously tested for applications with data from the BEAR and IMAGE magnetometer arrays. A combined application of the SECS and complex image method (CIM) for geomagnetic induction studies was introduced. The June 26, 1998 event was investigated.

**IV)** GIC and magnetic data from northern Europe with ionospheric equivalent currents derived applying the SECS method were used to investigate ionospheric drivers of GIC during the April 6-7, 2000 geomagnetic storm. A solid component of the work was the investigation by Huttunen et al. (2002) where the entire Sun - solar wind - magnetosphere - ionosphere chain was studied for this storm. Additional conclusions were drawn using statistics derived from the GIC measurements in the Finnish pipeline.

**V)** The SECS method was applied to the magnetic field separation problem. Using synthetic ionospheric current models and image currents mimicking the Earth response, the new method was tested for applications with BEAR and IMAGE magnetometer arrays. Data from the BEAR period were used to separate the field for real events and the results were discussed.

The core of the thesis is composed of the attached five papers. The purpose of the introductory part of the thesis is to give the basic background relevant for understanding the topics discussed in the papers and to relate the work made in them to a "bigger" context of solid Earth and solar-terrestrial physics. Repeating text from the attached papers is avoided whenever reasonable, and the reader is preferably referred to an appropriate paper for more detailed discussions.

In Chapter 1, general phenomena of space weather and its role for our environment are briefly outlined and some of the non-ground effect aspects are discussed. However, the emphasis of the chapter is mainly on a relatively low-level introduction to the ground induction effects of space weather. Light is shed on the basic physics behind the effects and on how different technological systems are affected. In Chapter 2, the general theoretical basis and the modeling artillery used in quantitative GIC investigations are pre-

sented. The aim of the chapter is to furnish a rather complete treatment of the physics relevant for GIC. This means, that if the basic relation relevant to our discussion is not derived in one of the attached publications, the derivation is given here starting from first principles. In the last section of the chapter, a unification of the mathematical methods applicable for GIC investigations is introduced. In Chapter 3 the characteristics of the GIC phenomena are discussed in the context of the work done in the thesis. Though the two sections of the chapter, one on geoelectric fields and another on ionospheric currents, are rather closely related, a separate treatment is pursued for clarity. Finally, in Chapter 4 the theses of the work are given and the challenges for future GIC investigations are briefly discussed.

This thesis work was carried out at the Geophysical Research Division (GEO) of the Finnish Meteorological Institute (FMI). A number of people deserve my sincere gratitude. First I would like to thank Professors Risto Pellinen and Tuija Pulkkinen, the former and the acting Director of GEO, respectively, as well as Prof. Erkki Jatila and Dr. Petteri Taalas, the former and the present Director General of FMI, respectively, for providing excellent working conditions. The successful completion of the work would not have been possible without the talented and effective supervisor Dr. Ari Viljanen, whose MatLab programs did great deal of the work presented in this thesis. The unofficial supervisors Drs Olaf Amm and Risto Pirjola have put lot of work (along with A. Viljanen) into discussing numerous theoretical and other issues related to the thesis and in correcting the worst errors in my grammar. R. Pirjola is acknowledged also for being a flexible and encouraging head of the Space Physics Research Group and for saying: "next is the last" - after the "last" one in numerous places for sufficient number of times. Besides the colleagues in Finland and elsewhere that I have had the chance to work with, I would like to acknowledge Gasum Oy and Fingrid Oyj, the owners of the Finnish natural gas pipeline and the high-voltage transmission system, respectively, for their continuous support for the Finnish GIC research. The reviewers of the thesis, Prof. Wolfgang Baumjohann and Dr. Jürgen Watermann are gratefully acknowledged. The work was financially supported by the Academy of Finland.

There is also life beyond work, though the boundary between the work and "other things" can sometimes be rather fuzzy. My lovely partner, Katja "Muori" Mikkonen knows only too well what this means. She is the one who bore evenings in the sound of typing and angry curses. Muori, I cannot thank you enough for your patience and support. The greatest rock'n'roll band in the history of space science, Geodynamo, is acknowledged for giving tinnitus and unforgettable moments on the stage. I am also indebted to Mega Duty



weightlifting sessions with Ari-Matti Harri that were the extra piece of fun that kept me going both mentally and physically. Finally, I would like to thank my family and friends who along with Muori form the strongest and the most important building block of my life.

A. Pulkkinen  
Helsinki, Finland  
June, 2003



# Notations

Below are listed the symbols and acronyms used in the work. Vector quantities are denoted by bold letters. SI units are used throughout the work.

- E** electric field in the spatial domain
- e** electric field in the spectral domain
- B** magnetic field in the spatial domain.
- b** magnetic field in the spectral domain.
- j** electric current density
- J** electric sheet current density
- J<sub>cf</sub>** curl-free sheet currents
- J<sub>df</sub>** divergence-free sheet currents
- J<sub>eq</sub>** equivalent sheet currents
- I** set of scaling factors of the spherical elementary systems
- t* time
- $\sigma$  electrical conductivity
- $\mu_0$  permeability of the free space
- $\epsilon_0$  permittivity of the free space
- $R_e$  radius of the Earth
- $Z$  spectral impedance
- $Z_{ij}^{int}$  internal impedance of a transmission line
- $R_{ij} = Re(Z_{ij}^{int})$
- $Z_p$  impedance per unit length of a pipeline
- $Y_p$  admittance per unit length of a pipeline
- $I_{ij}^n$  current along a transmission line
- $I_i^e$  earthing current
- $p$  complex skin depth

BEAR Baltic Electromagnetic Array Research

CIM complex image method

DSTL distributed source transmission line

GIC geomagnetically induced current

IMAGE International Monitor for Auroral Geomagnetic Effects

P/S pipe-to-soil

SECS spherical elementary current system

SVD singular value decomposition

# Contents

<b>Preface</b>	<b>i</b>
<b>Notations</b>	<b>vii</b>
<b>1 Introduction</b>	<b>3</b>
1.1 The role of space weather for our environment . . . . .	3
1.2 Ground induction effects of space weather . . . . .	6
1.2.1 Physical basis . . . . .	6
1.2.2 Technological impacts . . . . .	10
<b>2 Theoretical framework</b>	<b>15</b>
2.1 Derivation of ionospheric equivalent currents . . . . .	16
2.1.1 Separation of the ground disturbance magnetic field into external and internal parts . . . . .	24
2.2 Computation of the ground geoelectric field . . . . .	26
2.2.1 Computation via surface magnetic field . . . . .	28
2.2.2 Computation using a known ionospheric current system	35
2.3 Computation of geomagnetically induced currents . . . . .	39
2.3.1 Discretely grounded systems . . . . .	39
2.3.2 Continuously grounded systems . . . . .	45
2.4 Unification of the methods for practical applications . . . . .	46
<b>3 Characteristics of intense GIC events</b>	<b>49</b>
3.1 Properties of intense meso-scale geoelectric fields . . . . .	49
3.2 Properties of ionospheric currents causing intense geoelectric fields and the linkage to large-scale magnetospheric phenomena	54
<b>4 Discussion</b>	<b>61</b>
4.1 Theses of the work . . . . .	61

4.2 New challenges . . . . . 62

# Chapter 1

## Introduction

### 1.1 The role of space weather for our environment

There is weather also in space. Although there are on average only few particles per cubic centimeter in the solar wind driving the weather in space, the vast size of the system and the complex coupling mechanisms make this nearly vacuum environment very dynamic and capable to affect our everyday life. Physical processes driving space weather are linked by the chain of causal connections starting from processes on the Sun. Quoting James A. Van Allen, after whom the two radiation belts surrounding the Earth are named, from the foreword of Carlowicz and Lopez (2002): "Space weather is attributable to highly variable outward flow of hot ionized gas (a weakly ionized "plasma" at a temperature of about 100.000 degrees Kelvin, called the solar wind) from the Sun's upper atmosphere and to nonthermal, sporadic solar emissions of high-energy electrons and ions and electromagnetic waves in the X-ray and radio portions of the spectrum". The coupling of the flow of solar wind and nonthermal emissions to the Earth's magnetosphere, coupled itself to the ionosphere, is obtained via several different physical processes. The processes relevant in the context of this thesis will be reviewed and discussed below.

The most famous definition for space weather was formulated in 1994 during the birth of the US National Space Weather Program (Robinson and Behnke, 2001). It reads as follows:

*Space weather refers to conditions on the Sun and in the solar wind, magnetosphere, ionosphere, and thermosphere that can influence the performance and reliability of space-borne and ground-based technological systems and can*

*endanger human health. Adverse conditions in the space environment can cause disruption of satellite operations, communications, navigation, and electric power distribution grids, leading to a variety of socioeconomic losses.*

When extended through the notification that mankind can also benefit from (instead of solely suffer from it) good space weather, i.e. with beautiful sights of auroras, the definition is quite comprehensive and describes well the basic meaning of space weather. The important point to realize is that space weather is a concept that rather than just being another term for solar-terrestrial physics (STP), combines both technological and scientific aspects of our near space environment.

Highlights of some of the adverse effects that space weather has on systems and the mechanisms behind the effects are presented in Fig. 1.1. These include single-event upsets in the spacecraft electronics caused by high energy protons, electron induced spacecraft surface and internal charging leading to discharge currents, solar panel degradation due to particle bombardment, tissue damages due to particle radiation, increased atmospheric drag experienced by low orbit spacecraft, disturbances in HF communication and navigation systems caused by the irregularities in the ionosphere, cosmic ray induced neutron radiation at airline flights, geomagnetically induced currents (GIC) in long conductor systems on the ground caused by rapidly varying ionospheric currents and lastly one of the hottest topics in geophysics, the possible modulation of the neutral atmospheric weather by space weather. For more complete listings see e.g. Lanzerotti et al. (1999); Feynman (2000); Koskinen et al. (2001); Lanzerotti (2001).

The discovery of the telegraph system in the 19th century, was the turning point after which the near space phenomena begun to have direct adverse effects on man's daily life. Positive aspects of the phenomena date farther back in time. The first records of auroras originate from ancient times (fairly continuous from 560 AD onward) from Eastern Asia and Europe (Pang and Yau, 2002). It is obvious, although not unambiguously recorded, that auroras were observed also before. The number of potentially vulnerable systems increased rapidly in the beginning of the 20th century: Wireless communication applying long wavelength radio transmissions, complex high-voltage power transmission networks and long trans-Atlantic telecommunication cables, and eventually orbiting spacecraft were all found to be affected by space weather. Thus there appeared growing need for deeper understanding of the phenomena and even for the establishment of services providing space weather related information to the operators of the affected technological systems. In the 1990's, the enhancement of near space environ-



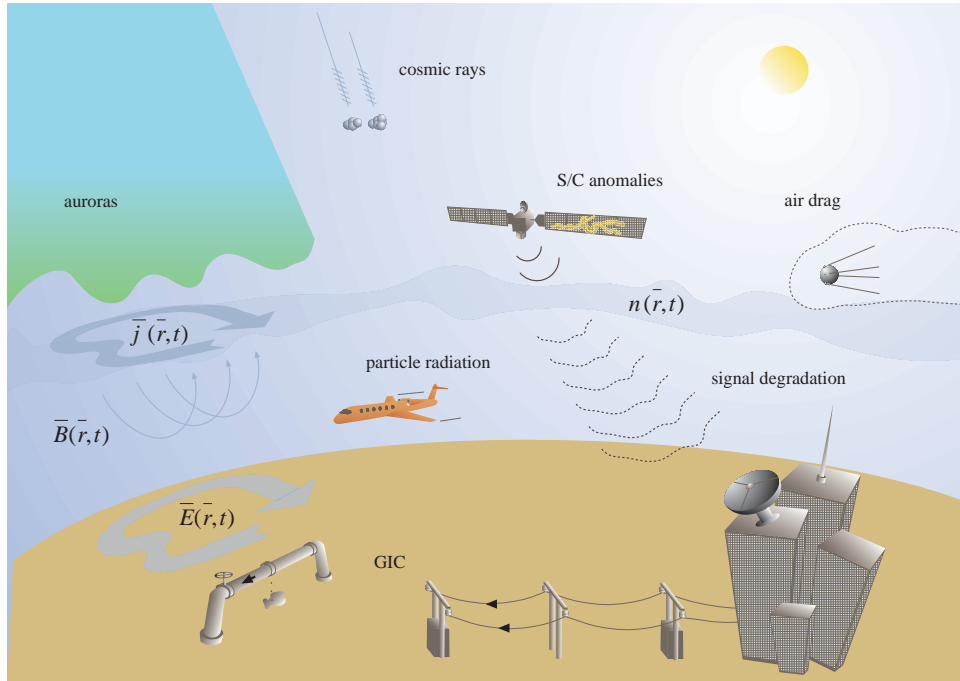


Figure 1.1: Highlights of effects of space weather. See text for details.

ment monitoring capabilities and increasing quantitative knowledge about the solar-terrestrial physics enabled the establishment of the pilot space weather services. The most extensive and the best known of such services is the Space Environment Center (SEC) operated by the National Oceanic and Atmospheric Administration (NOAA) and by the US Air Force at Boulder, Colorado, USA (see [www.sec.noaa.gov](http://www.sec.noaa.gov)). The strong financial investment, partially due to military driving, to the US space weather activities has ensured that although a number of smaller service centers have been put up recently around the world, the leading space weather related capabilities are still located in North America (e.g., Robinson and Behnke, 2001; Withbroe, 2001). However, the fact that space weather is affecting us and the increasing pressure on institutes carrying out solar-terrestrial physics research to show the practical benefit of their work is making the space weather topic increasingly popular in the scientific community throughout the world. For example, the European Space Agency (ESA) has recently become actively involved in space weather related issues (Daly and Hilgers, 2001) and is presently creating foundations for a common European space weather pro-

gram via targeted pilot services. Space weather related research efforts have also started within the European Union. Consequently, the US lead in space weather related research and services is likely to narrow in the future, and more importantly, the present international efforts guarantee that the recent trend of growing popularity of space weather will remain.

## 1.2 Ground induction effects of space weather

### 1.2.1 Physical basis

After installation of the first telegraph systems in the 1830's and 1840's, it was noticed that from time to time there were electric disturbances driving such large "anomalous" currents in the system that the transmissions of the messages was extremely difficult while at other times no battery was needed for the operation (e.g., Barlow, 1849; Prescott, 1866). For example, the famous September 1859 geomagnetic storm (term introduced by Alexander von Humboldt in the 1830's) produced widespread disturbances in the telegraph systems in North America and Europe. The disturbances coincided with the solar flare observations of Carrington and auroral observations all over the world (Loomis, 1859; Carrington, 1860) and led to speculations about the possible connection between these phenomena. However, the physical explanation remained unclear for the next half century. Eventually, in the late 19th century the experimental evidence build up and confirmed the relation between the solar, auroral and ground magnetic phenomena. During the First Polar Year (1882-1883) scientists defined *magnetic storms* as intense, irregular variations of the geomagnetic field which occur as a consequence of solar disturbances (e.g., Kamide, 2001). The work by Birkeland, Størmer and Chapman, although differing in details, suggested that the origin for variations of the ground magnetic field was in the electric currents in space and that the currents in turn were created by the interaction between the magnetic field of the Earth and particles streaming from the Sun. The beginning of the space age in the 1950's made direct observations of the space environment possible and since then the important discoveries and confirmations of earlier theories followed quickly each other: The existence of the radiation belts, field-aligned currents coupling the ionosphere to the magnetosphere, solar wind, solar sources for geomagnetic disturbances (flares, coronal mass ejections, coronal holes). The new information from the space and from the growing network of ground magnetic observatories finally made it possible to understand the basics of the the origins and mechanisms for ground effects of space weather (for a popular presentation see

e.g., Carlowicz and Lopez, 2002).

Besides the advances in early space physics, significant progress was also made in understanding the electromagnetic induction of geomagnetic origin (geomagnetic induction) inside the Earth, the ultimate reason for the existence of the currents in ground conductor systems. The basic foundations for advanced induction studies were laid by Faraday, who discovered in 1830's that time varying magnetic fields create currents in electrically conducting materials. The first quantitative measure for geomagnetic induction was given by Schuster (1889), who investigated magnetic field related to diurnal variations and found that a small portion of the field was of internal origin, i.e. caused by the currents induced within the Earth. Also in the induction studies the great advances were made after the turn of the 19th century, the work being focused on dealing with increasingly complicated ground conductivity structures (e.g., Lahiri and Price, 1938). However, besides to somewhat cumbersome scale analogue models (e.g., Frischknecht, 1988), the work with realistic three-dimensional conductivity structures has not been possible prior to the advent of large computational power.

Noteworthy is that the main motivation in the majority of the geomagnetic induction studies has been in deducing the electrical properties of the Earth from the measured magnetic field variations. Though the basic source morphology has been investigated (e.g., Mareschal, 1986), the actual source processes for these variations has been of relatively little interest. Thus until the present days, there has been a substantial gap between the geomagnetic induction and space physics communities regardless the physical connection between the two. Space weather is a link between the disciplines, as can be seen from the work at hand.

By merging the accomplishments made in the solid Earth and solar-terrestrial physics, the way how solar activity can influence the performance of ground based systems can be depicted. The process can be divided into six steps along the chain of physical connections (see Fig. 1.2):

1.) Plasma processes in the Sun cause ejection of material that has the capability of driving geomagnetic activity. From the viewpoint of the strongest ground effects, coronal mass ejections (CME) and coronal holes with high speed solar wind streams are the two most important categories (e.g., Tsurutani, 2001).

2.) The propagation of the magnetized plasma structures in the interplanetary medium. From the space weather viewpoint, it is noteworthy that due to absence of remote sensing techniques, the evolution of the structures is

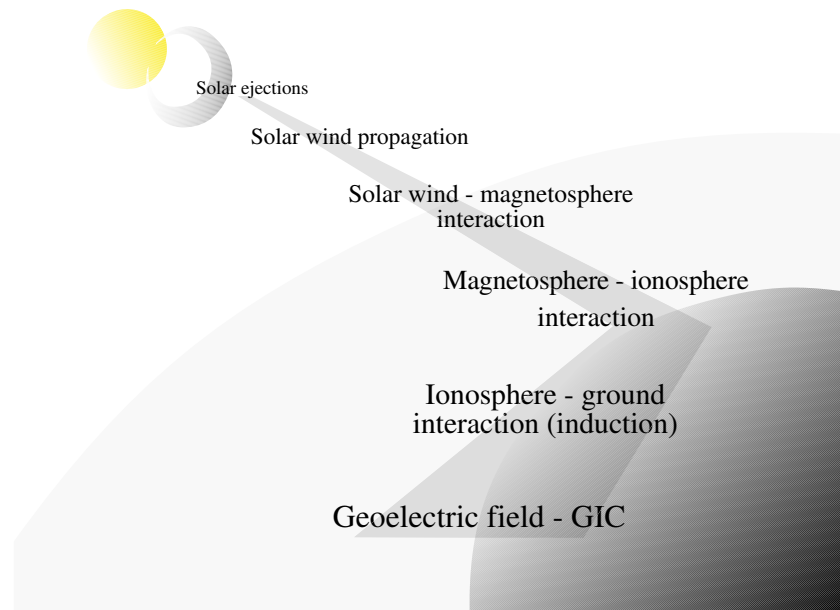


Figure 1.2: Six steps of space weather chain from the Sun to the ground.

very difficult to estimate.

3.) Interaction between the solar wind (or structures within) and magnetosphere (Fig. 1.3). Here the dominant factor for determining the geoeffectiveness of the structure is the orientation of the solar wind magnetic field, i.e. how much southward the field is. The energy feed into the magnetosphere is highest during strong reconnection of the solar wind and the magnetospheric magnetic fields. Increased energy input to the system sets the conditions for dynamic changes in the magnetospheric electric current systems. One of such dynamic changes are magnetic storms which are characterized by enhanced convection of the magnetospheric plasma and enhanced ring current circulating the Earth (see e.g., Tsurutani and Gonzalez, 1997).

4.) Magnetosphere-ionosphere interaction. The closure of the magnetospheric currents systems goes via polar regions of the ionosphere. Correspondingly, dynamic changes in the magnetospheric current systems couple to the dynamics of the ionosphere. An important class of dynamic variations are auroral substorms which are related to loading-unloading processes in the tail of the magnetosphere (e.g., Kallio et al., 2000). During auroral

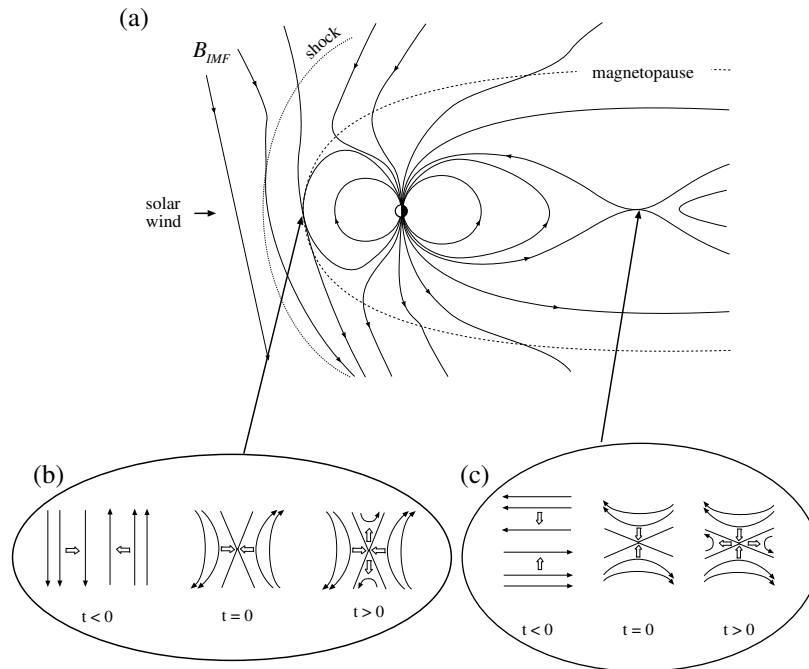


Figure 1.3: (a) Interaction process between the solar wind magnetic field  $B_{IMF}$ , i.e. interplanetary magnetic field and Earth's magnetic field. (b) Reconnection between the magnetic field of these two regions changes the field topology and transports energy into the magnetosphere. (c) Another reconnection site in the night-side magnetosphere separates the interplanetary and the magnetospheric magnetic fields. Figure adopted from Tanskanen (2002).

substorms particles injected from the tail of the magnetosphere are seen in the ionosphere in terms of auroras and rapid changes in the auroral current systems. Although some of the basic features are understood, the details of the storm and substorm processes as well as the storm/substorm relationship are one of the most fundamental open questions in the solar-terrestrial physics (for a review see e.g., Kamide, 2001).

5.) Rapid changes of the ionospheric and magnetospheric electric currents cause variation in the geomagnetic field which according to Faraday's law of induction induce an electric field which drives an electric current in the sub-surface region of the Earth. The nature of this geoelectric field is dependent

on the characteristics of the ionospheric-magnetospheric source and on the conductivity structure of the Earth. As a rule of thumb, the magnitude of the geoelectric field increases with increasing time derivatives of the ground magnetic field and with decreasing ground conductivity.

6.) Finally, the geoelectric field drives currents within conductors at and below the surface of the Earth. The magnitude and distribution of the currents are dependent on the topology and electrical characteristics of the system under investigation. The induced currents flowing in technological systems on the ground are called *geomagnetically induced currents* (GIC).

### 1.2.2 Technological impacts

The first technological impacts of space weather were seen on telegraph systems where disturbances in signals and even fires at telegraph stations were experienced (Harang, 1941). However, in principle all conductors can be influenced by GIC. Due to the relatively small magnitudes of geoelectric fields, with maximum observed values being of the order of 10 V/km (Harang, 1941), only spatially extended systems can be affected.

After the telegraph equipment, the next category of technological conductor systems seen to be affected were power transmission systems (the first report by Davidson, 1940). Regarding economic impacts, industrial interests and the number of studies carried out, the effects on power transmission systems are, to the present knowledge, the most important category of space weather effects on the ground. Solely the impact of the great March 1989 storm on power systems in North America was greater than reported in other systems altogether at all times (e.g., Czech et al., 1992; Kappenman, 1996). Barnes and Van Dyke (1990) estimated that a blackout in the Northeast US for 48 hours would cost as an unserved electricity and replacements of the damaged equipment from 3 to 6 billion US dollars.

In power transmission systems, the primary effect of GIC is the half-cycle saturation of high-voltage power transformers (e.g. Kappenman and Albertson, 1990; Molinski, 2002). The typical frequency range of GIC is 1 - 0.001 Hz (periods 1 - 1000 s), thus being essentially direct current (dc) for the power transmission systems operating at 60 Hz (North America) and 50 Hz (Europe). (Quasi-)dc GIC causes the normally small exciting current of the transformer to increase even to a couple orders of magnitude higher values, i.e. the transformer starts to operate well beyond the design limits (see Fig. 1.4). The saturated transformer causes an increase of the reactive power consumed by the transmission system, ac character of the

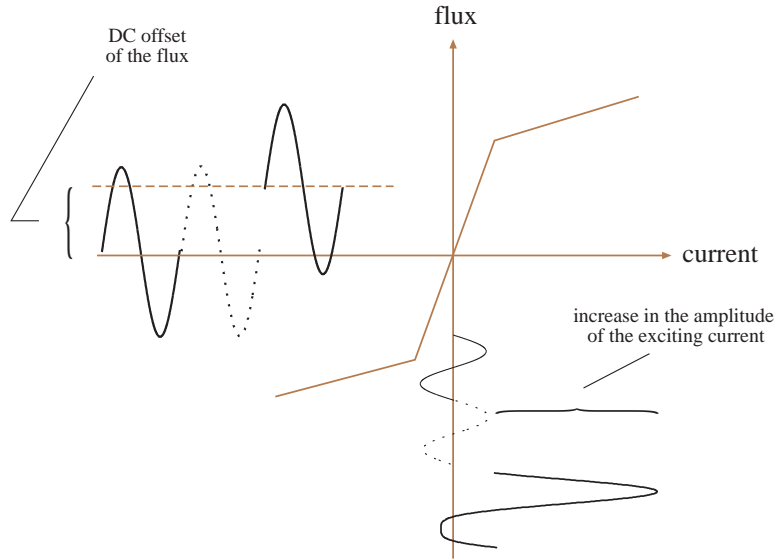


Figure 1.4: Simplified illustration of the saturation of the transformer. When the magnetic flux inside the transformer is offset by the (quasi-)dc GIC, the transformer starts to operate in the non-linear portion of the magnetization curve, i.e. a small increase in the flux requires a large increase in the exciting current.

power transmission which means that the real power available in the system is decreasing. Another effect of the saturated transformer is that the 50 or 60 Hz waveform is distorted, i.e. the higher harmonic content in the electricity increases. Harmonics introduced to the system decrease the general quality of the electricity, and may cause false trippings of protective relays designed to switch the equipment off in the case of erratic behavior of the system. Trippings of the static VAR compensators (employed to deal with the changing reactive power consumption) started the avalanche that finally led to the collapse of the Canadian Hydro-Québec system on March 13, 1989 (e.g., Boteler et al., 1998; Bolduc, 2002).

Also more advanced telecommunication cables than single-wire telegraph systems have been affected. The principal mode of failure for these systems are via erroneous action of power apparatus that are used for energizing the

repeaters of the cable (Root, 1979). This is why even modern optic fiber cables could be affected (Medford et al., 1989). The best known incidents are the disruption of communications made via TAT-1, the cross-Atlantic (from Newfoundland to Scotland) communication cable in February 1958 (Anderson, 1978) and the shutdown of the AT&T L4 cable running in the mid-western US in August 1972 (Anderson et al., 1974). In addition to communication problems in February 1958, there was a blackout in the Toronto area due to a power system failure (Lanzerotti and Gregori, 1986).

Effects of GIC on pipelines have been of concern since the construction of the 1280 km long Trans-Alaskan pipeline in the 1970's (Lanzerotti and Gregori, 1986). The flow of GIC along the pipeline is not hazardous but the accompanying pipe-to-soil (P/S) voltage (see Fig. 1.5) can be a source for two different types of adverse effects (e.g., Brasse and Junge, 1984; Boteler, 2000; Gummow, 2002). The more harmful effect is related to the currents driven by the P/S voltage variations. If the coating, used to insulate the pipeline steel from the soil, has been damaged or the cathodic protection potential used to prevent the corrosion current is exceeded by the P/S voltage, the corrosion rate of the pipeline may increase. However, estimates about the time that it takes from the geomagnetic disturbances to seriously damage vary quite a lot and no publicly reported failures due to GIC-induced corrosion exist (e.g., Campbell, 1978; Henriksen et al., 1978; Martin, 1993). Thus if the pipeline is properly protected against the corrosion, it is likely that the second and the most important effect of GIC are the problems in measuring the cathodic protection parameters and making control surveys during geomagnetically disturbed conditions.

Although railway systems also have long electrical conductors, it seems that malfunctions due to geomagnetic disturbances are very rare. The only reported incident is from Sweden, where during a magnetic storm in July 1982 traffic lights turned unintentionally red (Wallerius, 1982). Erroneous operation was explained by the geomagnetically induced voltage that had annulled the normal voltage, which should only be short-circuited when a train is approaching leading to a relay tripping. It is, of course, possible that some of past "unknown" railway disturbances have in fact been caused by GIC.

In general, GIC has been a source for problems in technological systems on the ground since the mid 19th century, the number of reports being roughly a function of the sunspot number and global geomagnetic activity (Fig. 1.6). The number of technological conductor systems is inevitably increasing and some of these systems will be built in regions where they can be affected by GIC. Thus, it is quite obvious that GIC will be of concern for



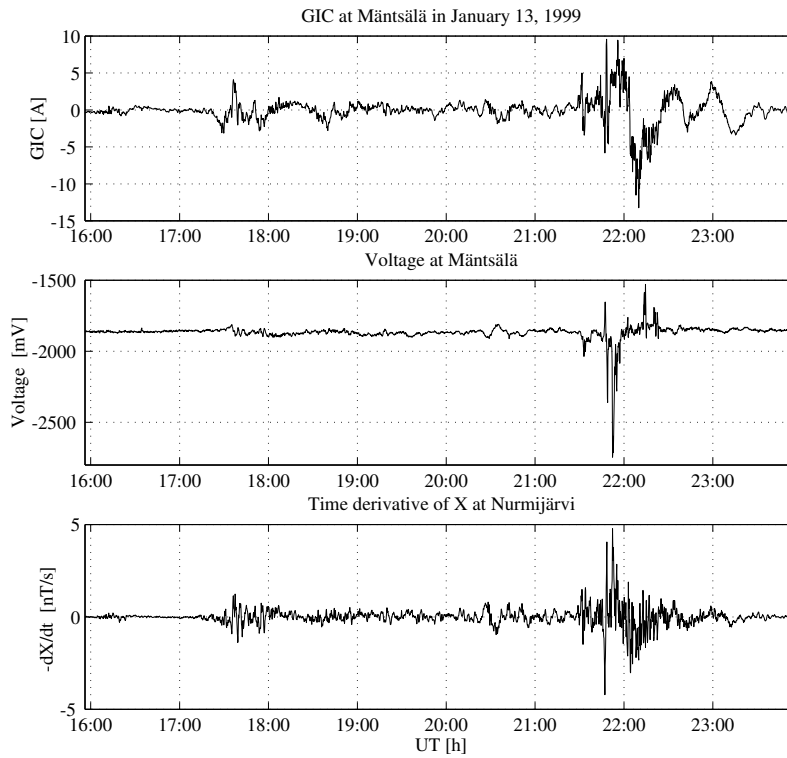


Figure 1.5: GIC and pipe-to-soil (P/S) voltage measured in the Finnish pipeline at the Mäntsälä pipeline section and the time derivative of the north component of the magnetic field measured at the Nurmijärvi Geophysical Observatory on January 13, 1999. Note the offset of the P/S voltage zero level due to the cathodic protection, and the close relation between the time derivative of the magnetic field and GIC.  $-dX/dt$  has roughly the same behavior as the eastward geoelectric field.

system operators also in the future. For more complete reviews on historical facts and technological impacts of GIC see for example Lanzerotti and Gregori (1986); Boteler et al. (1998); Boteler (2001a); Pirjola (2002).

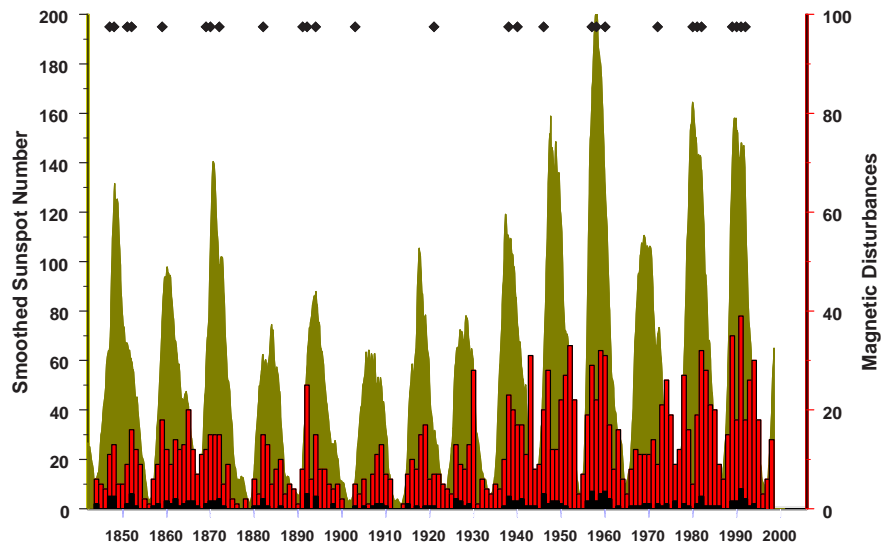


Figure 1.6: Solar and geomagnetic activity and the reported occasions (diamonds) of ground induction effects of space weather. The solar activity is depicted by the sunspot number (olive curve). Red bars indicate the number of geomagnetic disturbances having the 24-hour global geomagnetic activity  $aa^*$  index above 60 nT, and black bars indicate the number of disturbances having  $aa^*$  index above 120 nT. Figure adopted from Boteler et al. (1998); Jansen et al. (2000).

## Chapter 2

# Theoretical framework

The modeling of GIC in specific technological systems is usually divided into two independent steps:

- 1.) Calculation of the surface horizontal geoelectric field based on the knowledge of the ionospheric source currents and of the ground conductivity structure. As a sub-step, we may need to derive the ionospheric source current first.
- 2.) Calculation of GIC based on the knowledge of the surface geoelectric field and of the topology and electrical parameters of the technological conductor system under investigation.

The independence of these two steps is based on the assumption that the inductive coupling between the Earth and the technological conductor system can be neglected. This may seem to be quite a severe assumption at first glance but as will be seen below, the coupling is not very strong at the frequencies of our interest ( $< 1$  Hz) and is thus a second order effect from the GIC modeling point of view. If the coupling is not neglected, the treatment becomes complex and very restricting assumptions, like an infinite length of the conductor, are needed to keep the problem mathematically tractable. This is the basic problem of GIC modeling, and perhaps more generally in all geophysical modeling: One is forced to search for pragmatic approaches where a variety of quite substantial approximations are made. However, in the GIC modeling the needed approximations are relatively feasible. For example, the locality of the studies justifies the flat-Earth assumption, and integration of the surface electric field made in computing GIC results in

that only meso-scale ( $\sim 100$  km) fields and ground conductivity structures are of interest to us. Furthermore, any higher accuracy than one ampere for the GIC amplitude is not needed. Getting the overall picture is far more important. This is explained in greater detail in Chapter 3 where the characteristics of intense GIC events are discussed.

Assuming that the decomposition of the GIC modeling problem can be made as stated above, we approach the two steps as separate problems. In Sections 2.1 and 2.2 we consider the *geophysical step*, i.e. determination of the ionospheric source currents and the calculation of the surface geoelectric field, respectively. In Section 2.3 we treat the *engineering step*, i.e. the calculation GIC in different technological systems.

## 2.1 Derivation of ionospheric equivalent currents

Ionospheric equivalent currents are a convenient way to model the ionospheric source from the geomagnetic induction viewpoint. Although they are not identical to the true three-dimensional ionospheric current system, they produce the same magnetic effect at the surface of the Earth as the true system. Examples of the usage of equivalent currents in induction studies will be seen later on in Chapter 3. First, however, we see how ionospheric equivalent currents are determined using ground magnetic data.

If the ionosphere were immediately above the surface of the Earth and the geometry were Cartesian, the equivalent currents  $\mathbf{J}_{eq}$  (A/m) situated on an infinitely thin sheet, could be obtained just by rotating the ground horizontal magnetic field vector 90 degrees clockwise and by multiplying with  $2/\mu_0$  where  $\mu_0$  is the permeability of the free space. However, if the standard approximation, regarding the ionosphere as a two-dimensional spherical shell at the 110 km height, is used, the situation is more complex and more sophisticated methods are required.

A number of methods, like spherical harmonic (Chapman and Bartels, 1940), spherical cap harmonic (Haines, 1985) and Fourier (Mersmann et al., 1979) methods, have been applied to the determination of the ionospheric equivalent currents. However, all of them suffer from drawbacks that can be avoided by applying the spherical elementary current system (SECS) method. Furthermore, as will be seen in Section 2.2.2, the SECS method can be combined with the complex image method used for the quick determination of the electromagnetic field at the surface of the Earth. This feature is of significant importance for GIC-related induction studies since it permits the utilization of realistic ionospheric sources. For a more detailed

discussion on advantages of the SECS method compared to the traditional methods, see the introduction of Paper III. The mathematical foundations of the SECS method were established by Amm (1997); Amm and Viljanen (1999). Below we briefly outline the method and its usage with the geomagnetic data.

In the SECS method, we compose ionospheric sheet currents from the divergence-free and curl-free parts of the vector field. This is similar to representing the current by other elementary systems like magnetic dipoles (e.g., Weaver, 1994, p. 12-15), or by current loops having an east-west and north-south directed ionospheric part and closing in the magnetosphere as in Kisabeth and Rostoker (1977). However, elementary systems used here are more fundamental in that they by their basic structure represent the divergence and the curl of the horizontal current system. Furthermore, as will be seen below, only the divergence-free part of the currents is needed to represent equivalent currents, thus reducing the number of degrees of freedom by a factor of two.

According to the *Helmholtz theorem*, any vector field can be decomposed into divergence-free (df) and curl-free (cf) parts (see e.g. Arfken and Weber, 1995, p. 92-97). Or vice versa, if we know the divergence and the curl of a vector field and its normal component over the boundary, the field itself is uniquely determined. This allows us to represent the ionospheric currents, assumed to flow in an infinitely thin spherical shell of radius  $R_I$  (measured from the Earth's centre), as

$$\mathbf{J}(\mathbf{s}) = \mathbf{J}_{df}(\mathbf{s}) + \mathbf{J}_{cf}(\mathbf{s}) \quad (2.1)$$

where

$$\nabla_h \cdot \mathbf{J}_{df}(\mathbf{s}) = 0 \quad (2.2)$$

$$[\nabla \times \mathbf{J}_{cf}(\mathbf{s})]_r = 0 \quad (2.3)$$

and

$$[\nabla \times \mathbf{J}_{df}(\mathbf{s})]_r = u(\mathbf{s}) \quad (2.4)$$

$$\nabla_h \cdot \mathbf{J}_{cf}(\mathbf{s}) = v(\mathbf{s}) \quad (2.5)$$

where  $\mathbf{s}$  is the vector giving coordinates on the shell (see Fig. 2.1) and  $u$  and  $v$  are the source terms. Note that in Eqs. (2.2)-(2.5) the radial derivative of the sheet current is not well defined and thus the divergence is taken only for the horizontal components ( $\nabla_h$ ) and only the radial component of the

curl is taken into account. Physically,  $v$  in Eq. (2.5) can be interpreted as a field-aligned current density ( $\text{A}/\text{m}^2$ ).

Now let us seek solutions for  $\mathbf{J}_{df}$  and  $\mathbf{J}_{cf}$  in Eq. (2.1) using conditions (2.2)-(2.5). The problem can be treated in separate parts; we first deal with  $\mathbf{J}_{cf}$ . Generally, using Green's functions we may write

$$\mathbf{J}_{cf}(\mathbf{s}) = \int_S \mathbf{G}_{cf}(\mathbf{s}, \mathbf{s}_0) v(\mathbf{s}_0) d\mathbf{s}_0 \quad (2.6)$$

where

$$\nabla_h \cdot \mathbf{G}_{cf}(\mathbf{s}, \mathbf{s}_0) = \delta(\mathbf{s} - \mathbf{s}_0) - \frac{1}{4\pi R_I^2} \quad (2.7)$$

and  $\delta$  is a standard Dirac delta function. By taking the divergence of (2.6) and substituting Eq. (2.7) we may verify that the condition (2.5) is fulfilled if we require that the total three-dimensional current system is divergence-free (what comes in, must go out), i.e.

$$\int_S v(\mathbf{s}_0) d\mathbf{s}_0 = 0 \quad (2.8)$$

Relation (2.7) describes the elementary source for the curl-free part of the vector field in (2.1). Apart from the traditional point source seen for example in the treatment of the electrostatic problem (see e.g., Arfken and Weber, 1995, p. 510-512), we have an elementary source composed of both a point source at  $\mathbf{s}$  and a uniform outflow distributed over the surface  $S$  (See Fig. 2.2). The uniform outflow results in locality of the elementary source and is needed in spherical geometry to fulfill the divergence-free condition of a single source. Another choice for the elementary source could have been such that the inward and outward flows are at the antipoloidal points on the spherical ionosphere (Fukushima, 1976). However, this type of current system couples the opposite sides of the ionosphere and is not as general as the choice made here.

If we can solve  $\mathbf{G}_{cf}$  defined by (2.7) then we are able to compute  $\mathbf{J}_{cf}$  via Relation (2.6). The problem can be simplified by defining

$$\mathbf{G}_{cf}(\mathbf{s}, \mathbf{s}_0) = Q^{-1}(\mathbf{s}, \mathbf{s}_0) \mathbf{G}_{cf}^{el}(Q(\mathbf{s}, \mathbf{s}_0)\mathbf{s}) \quad (2.9)$$

where  $Q$  is an operator carrying out the changes between a common coordinate system having a pole at  $N$  (see Fig. 2.1) and a coordinate system having pole at  $\mathbf{s}_0$ . We denote the vector in the coordinate system having pole at  $\mathbf{s}_0$  by  $\mathbf{s}' = Q(\mathbf{s}, \mathbf{s}_0)\mathbf{s}$ . The explicit form of the operator  $Q$  will be given below. The basic idea in Eq. (2.9) is that by the rotation of the

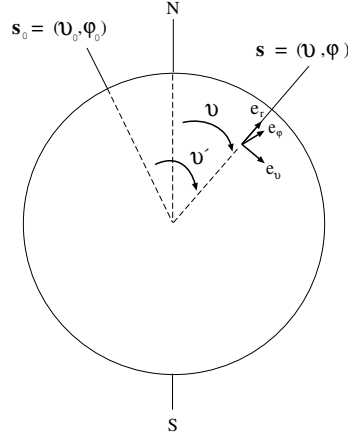


Figure 2.1: Coordinate system used in deriving spherical elementary current system method.

coordinate system we are able to reduce the determination of  $\mathbf{G}_{cf}$  to the determination of function of one variable, i.e. to determination of  $\mathbf{G}_{cf}^{el}(\vartheta')$ . We define  $\mathbf{s} = (\vartheta, \varphi)$  where  $\vartheta$  and  $\varphi$  are the polar and azimuth angles, respectively. Now in the coordinate system having pole at  $\mathbf{s}_0 = (\vartheta_0, \varphi_0)$  it is simple to show that Eq. (2.7) with the boundary condition  $\mathbf{G}_{cf}^{el}(\vartheta' = \pi) = 0$  is fulfilled by the function

$$\mathbf{G}_{cf}^{el}(\vartheta') = \frac{1}{4\pi R_I} \cot(\vartheta'/2) \mathbf{e}_{\vartheta'} \quad (2.10)$$

where  $\vartheta'$  is the angle between  $\mathbf{s} = (\vartheta, \varphi)$  and  $\mathbf{s}_0 = (\vartheta_0, \varphi_0)$  (see Fig. 2.1) and  $\mathbf{e}_{\vartheta'}$  is the unit vector in the coordinate system having pole at  $\mathbf{s}_0 = (\vartheta_0, \varphi_0)$ . Eq. (2.10) for  $\mathbf{G}_{cf}^{el}$  with the operator  $Q$  enables the computation of the general  $\mathbf{G}_{cf}$  in Eq. (2.9) and thus the evaluation of Eq. (2.6). The problem for the curl-free part is solved.

The divergence-free part  $\mathbf{J}_{df}$  is handled completely analogously to the curl-free case. We obtain

$$\mathbf{G}_{df}^{el}(\vartheta') = \frac{1}{4\pi R_I} \cot(\vartheta'/2) \mathbf{e}_{\varphi'} \quad (2.11)$$

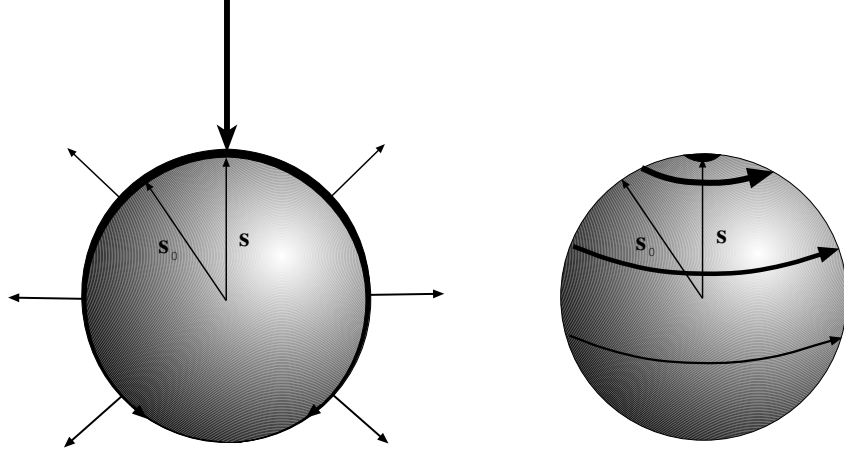


Figure 2.2: Left: Curl-free elementary system having a point source at  $\mathbf{s}$  and a uniform source distributed over  $S$ . Right: Divergence-free elementary system having a point source at  $\mathbf{s}$  and a uniform source distributed over  $S$ .

where again  $\mathbf{e}_{\varphi'}$  is the unit vector in the rotated coordinate system. Finally, we can write

$$\mathbf{J}_{df}(\vartheta, \varphi) = \frac{1}{4\pi R_I} \int_S u(\vartheta, \varphi) \cot(\vartheta'/2) Q^{-1} \mathbf{e}_{\varphi'} \sin(\vartheta_0) d\vartheta_0 d\varphi_0 \quad (2.12)$$

$$\mathbf{J}_{cf}(\vartheta, \varphi) = \frac{1}{4\pi R_I} \int_S v(\vartheta, \varphi) \cot(\vartheta'/2) Q^{-1} \mathbf{e}_{\vartheta'} \sin(\vartheta_0) d\vartheta_0 d\varphi_0 \quad (2.13)$$

where  $Q^{-1} = Q^{-1}(\vartheta, \varphi, \vartheta_0, \varphi_0)$ . Now the divergence and the curl of the vector field are known, and it follows from the Helmholtz theorem that using the spherical elementary current system representation in Eqs. (2.12) and (2.13), we can uniquely present any horizontal ionospheric current system.

To compute the currents, we need to know the sources  $u$  and  $v$  in Eqs. (2.12) and (2.13). The natural approach is to derive a relation between  $u$  and  $v$  and the magnetic field by applying the Biot-Savart law to the current distribution  $\mathbf{J}_{df} + \mathbf{J}_{cf}$  and to use the measured magnetic field to deduce the unknowns. However, as was shown by Fukushima (1976), the current system composed of the curl-free elementary system in Eq. (2.10) (left hand side in Fig. 2.2) does not cause any magnetic effect below the ionosphere. It means that in the auroral ionosphere where the inclination of the field-aligned currents is approximately 90 degrees, horizontal ionospheric currents satisfying the  $\nabla_h \times \mathbf{J} = 0$  condition do not cause any magnetic effect



on the ground. Further, it is shown in Paper V that the divergence-free elementary systems can fully explain the ground magnetic field variations caused by any three-dimensional ionospheric current system, independent of the inclination of the field-aligned currents. This is the ultimate reason why the divergence-free elementary currents are just equivalent currents ( $\mathbf{J}_{df} = \mathbf{J}_{eq}$ ). The complete three-dimensional current system cannot be deduced from the ground magnetic field only. Note that also the curl-free part of the currents can be deduced if the field-aligned current density (giving  $v(\vartheta, \varphi)$ ) is known (Amm, 2001).

It follows from the discussion above, that we only need the divergence-free elementary systems in this work. The vector potential related to  $\mathbf{G}_{df}^{el}(\vartheta')$  in Eq. (2.11) with the source  $u_0$  at  $\vartheta' = 0$  can be computed from

$$\mathbf{A}(\mathbf{s}') = \frac{\mu_0 u_0}{16\pi^2 R_I} \int_S \frac{\cot(\vartheta'_0/2)}{|\mathbf{s}' - \mathbf{s}'_0|} \mathbf{e}_{\varphi'} ds'_0 \quad (2.14)$$

where  $\mathbf{s}'$  is now a vector on a spherical shell having radius  $r < R_I$ . Integral (2.14) can be calculated by expanding the denominator using the addition theorem for Legendre functions and by eliminating the resulting series (see the details from the Appendix of Amm and Viljanen, 1999). The magnetic field of the elementary system in the polar coordinate system with pole at  $\mathbf{s}_0$  is obtained as  $\nabla \times \mathbf{A}$  and can be expressed as

$$B_{\vartheta'} = -\frac{\mu_0 u_0}{4\pi r \sin(\vartheta')} \left( \frac{\frac{r}{R_I} - \cos(\vartheta')}{\sqrt{1 - \frac{2r \cos(\vartheta')}{R_I} + \left(\frac{r}{R_I}\right)^2}} + \cos(\vartheta') \right) \quad (2.15)$$

$$B_{r'} = -\frac{\mu_0 u_0}{4\pi r} \left( \frac{1}{\sqrt{1 - \frac{2r \cos(\vartheta')}{R_I} + \left(\frac{r}{R_I}\right)^2}} - 1 \right) \quad (2.16)$$

where  $B_{\vartheta'} = \mathbf{B} \cdot \mathbf{e}_{\vartheta'}$  and  $B_{r'} = \mathbf{B} \cdot \mathbf{e}_{r'}$ . Eqs. (2.15) and (2.16) express the relation between the source  $u$  and the magnetic field  $\mathbf{B}$ . We thus can find  $\mathbf{J}_{df}$  in Eq. (2.12). Note that Eqs. (2.15) and (2.16) can be used to express the magnetic field in a continuum analogously to Eq. (2.12). The corresponding expression is the one for which the discretization is made below.

To look at the computation of the source  $u$  in practical applications, we first define a scaling factor  $I$  for the gridpoint of area  $A$  as

$$I = \int_A u(\vartheta_0, \varphi_0) \sin(\vartheta_0) d\vartheta_0 d\varphi_0 \quad (2.17)$$

Then, using a discrete elementary system grid, we can write for the magnetic field at the surface of the Earth

$$\mathbf{B}(\vartheta, \varphi) = \sum_{j=1}^M I_j \mathbf{T}_{df}^j(\vartheta, \varphi) \quad (2.18)$$

where  $\mathbf{T}_{df}^j$  are the geometric parts of Eqs. (2.15) and (2.16) ( $u_0$  omitted) with  $r = R_e$  (radius of the Earth) for  $M$  divergence-free elementary systems having poles at  $(\vartheta_j, \varphi_j)$ . Rotations to a common coordinate system using the operator  $Q^{-1}$  are not written here explicitly. By expanding Relation (2.18) for a discrete set of  $N$  measurements of the ground magnetic field at the locations  $(\vartheta_i, \varphi_i)$  we obtain the following set of equations

$$\begin{pmatrix} B_{\vartheta}(\vartheta_1, \varphi_1) \\ B_{\varphi}(\vartheta_1, \varphi_1) \\ B_r(\vartheta_1, \varphi_1) \\ \vdots \\ B_{\vartheta}(\vartheta_N, \varphi_N) \\ B_{\varphi}(\vartheta_N, \varphi_N) \\ B_r(\vartheta_N, \varphi_N) \end{pmatrix} = \begin{pmatrix} T_{\vartheta}^1(\vartheta_1, \varphi_1) & \dots & T_{\vartheta}^M(\vartheta_1, \varphi_1) \\ T_{\varphi}^1(\vartheta_1, \varphi_1) & \dots & T_{\varphi}^M(\vartheta_1, \varphi_1) \\ T_r^1(\vartheta_1, \varphi_1) & \dots & T_r^M(\vartheta_1, \varphi_1) \\ \vdots & & \vdots \\ T_{\vartheta}^1(\vartheta_N, \varphi_N) & \dots & T_{\vartheta}^M(\vartheta_N, \varphi_N) \\ T_{\varphi}^1(\vartheta_N, \varphi_N) & \dots & T_{\varphi}^M(\vartheta_N, \varphi_N) \\ T_r^1(\vartheta_N, \varphi_N) & \dots & T_r^M(\vartheta_N, \varphi_N) \end{pmatrix} \begin{pmatrix} I_1 \\ \vdots \\ I_M \end{pmatrix} \quad (2.19)$$

where on the left hand side we have the measured and on the right hand side the modeled field. The solution to (2.19) is obtained by finding the set of scaling factors  $\mathbf{I} = (I_1 \dots I_M)^T$  that reproduce the measured magnetic field. Due to the the usually under-determined character of the problem, i.e.  $M > N$ , a direct solution for example by means of normal equations would lead to numerical instabilities. Therefore, we use singular value decomposition (SVD). SVD stabilizes the least squares solution by searching the linear combination of solutions providing the smallest  $|\mathbf{I}|^2$ . Without going into further details, we note that in practice the stabilization in SVD is made by choosing the threshold  $\varepsilon$  for singular values related to different basis vectors of the decomposition. A larger value of  $\varepsilon$  implies a larger number of rejected basis vectors and in general a smoother solution for  $\mathbf{I}$ . For more details on SVD see Press et al. (1992, pp. 51-63). When  $\mathbf{I}$ , i.e  $u$ 's in terms of Relation (2.17), from Eq. (2.19) has been obtained, we are able to compute the divergence-free equivalent currents anywhere in the ionospheric plane. Note that the treatment can be given similarly also for the Cartesian geometry (see Amm, 1997). The resulting mathematical expressions are somewhat simpler in the Cartesian case, but due to the application of the SECS method

also to global problems (e.g., Huttunen et al., 2002), a treatment in spherical geometry was given here.

The magnetic disturbance caused by electromagnetic induction in the Earth is usually neglected in ionospheric studies. This leads to an over-estimation of the current amplitudes (Viljanen et al., 1995; Tanskanen et al., 2001) but the overall pattern of ionospheric equivalent currents is not severely miscalculated. However, some care about induction effects is needed when the SECS method is applied. If we set elementary currents only in the ionosphere, we implicitly assume that the disturbance field is purely of external origin. Because this is not exactly true, we do not solve the current amplitudes by using all three components of the ground magnetic field, but we only use horizontal components. This is acceptable, because the horizontal field can always be explained by using a purely ionospheric source (or as well, by a purely internal source). For a more detailed discussion on this matter see Paper III. The effect of induction is neglected in Papers III and IV (discussed in Chapter 3) where only the overall ionospheric equivalent current patterns are of interest and thus the full treatment of induction is not required. However, in Paper V, the SECS method is applied in a manner where also induction effects are taken into account. This will be discussed in Section 2.1.1.

To complete our discussion, we present the explicit form of the operator  $Q(\vartheta, \varphi, \vartheta_0, \varphi_0)$  carrying out the coordinate transformations (rotations) in Eqs. (2.12) and (2.13).  $Q$  is defined as

$$\begin{pmatrix} \mathbf{e}_{r'} \\ \mathbf{e}_{\vartheta'} \\ \mathbf{e}_{\varphi'} \end{pmatrix} = Q \begin{pmatrix} \mathbf{e}_r \\ \mathbf{e}_{\vartheta} \\ \mathbf{e}_{\varphi} \end{pmatrix} \quad (2.20)$$

$Q$  is composed of two operators  $T_{rot}$  and  $T_{sc}$ :

$$Q = T_{sc}^{-1}(\vartheta', \varphi') T_{rot}(\vartheta_0, \varphi_0) T_{sc}(\vartheta, \varphi) \quad (2.21)$$

where  $T_{sc}$  carry out the transformations between the spherical and the Cartesian coordinate systems and  $T_{rot}$  carries out the rotation of the coordinate system in the Cartesian coordinates. When using the standard relation between the coordinate systems,  $T_{sc}$  can be written as

$$T_{sc} = \begin{pmatrix} \sin(\vartheta) \cos(\varphi) & \cos(\vartheta) \cos(\varphi) & -\sin(\varphi) \\ \sin(\vartheta) \sin(\varphi) & \cos(\vartheta) \sin(\varphi) & \cos(\varphi) \\ \cos(\vartheta) & -\sin(\vartheta) & 0 \end{pmatrix} \quad (2.22)$$

where  $(\vartheta, \varphi)$  denotes the polar and azimuth angle of the point in the old coordinate system. Due to orthogonality of the transformations  $T_{sc}^{-1} = T_{sc}^T$ ,

and  $(\vartheta', \varphi')$  in  $T_{sc}^{-1}$  denotes the polar and azimuth angle of the point in the rotated coordinate system.  $T_{rot}$  can be written as

$$T_{rot} = \begin{pmatrix} \cos(\varphi_0) & \sin(\varphi_0) & 0 \\ -\cos(\vartheta_0)\sin(\varphi_0) & \cos(\vartheta_0)\cos(\varphi_0) & -\sin(\vartheta_0) \\ -\sin(\vartheta_0)\sin(\varphi_0) & \sin(\vartheta_0)\cos(\varphi_0) & \cos(\vartheta_0) \end{pmatrix} \quad (2.23)$$

where  $\vartheta_0$  and  $\varphi_0$  are polar and azimuthal angles of the rotation. Note the order of the rotation: 1.)  $\varphi_0$  is made counter-clockwise keeping the  $z$ -axis constant and 2.)  $\vartheta_0$  is made clockwise keeping the rotated  $x$ -axis constant. Now angles  $(\vartheta', \varphi')$  needed in  $T_{sc}^{-1}$  can be obtained by first computing

$$\begin{pmatrix} x' \\ y' \\ z' \end{pmatrix} = T_{rot}(\vartheta_0, \varphi_0)T_{sc}(\vartheta, \varphi) \begin{pmatrix} 1 \\ 0 \\ 0 \end{pmatrix} \quad (2.24)$$

and by computing then

$$\vartheta' = \arccos \frac{z'}{\sqrt{x'^2 + y'^2 + z'^2}} \quad (2.25)$$

$$\varphi' = \arctan \frac{y'}{x'} \quad (2.26)$$

Some attention should be paid to Eq. (2.26) when choosing the quadrant of the inverse tangent. Inverse rotations are carried out by the matrix  $Q^{-1} = Q^T$ .

### 2.1.1 Separation of the ground disturbance magnetic field into external and internal parts

This topic is discussed and treated in a complete manner in Paper V. Thus only a brief discussion about the relation of the field separation to GIC studies together with a very brief introduction to the application of the SECS method to the field separation problem, is given here.

As was noted above, also the magnetic effect arising from electromagnetic induction inside the Earth is contributing to the total field at the surface, i.e. the ground magnetic field is a superposition of external and internal parts. In some cases it is acceptable to neglect the internal effects, especially when only an overall behavior of the ionospheric equivalent current patterns is of interest. However, in some cases neglecting induction may

lead to erroneous interpretations or separated field components are needed as a starting point for the entire investigation. For example, depending on the individual situation, in the analysis of ionospheric electrodynamics, neglecting telluric effects may cause significant errors in the estimation of the ionospheric current intensity (Viljanen et al., 1995; Tanskanen et al., 2001), or even notable errors in the determination of some global magnetospheric indices like Dst (Häkkinen et al., 2002). Also, the ratio of the internal and external components contains information about the underlying ground conductivity structure (e.g., Berdichevsky and Zhdanov, 1984, p. 191). Methods applied to the estimation of the Earth's conductivity structure require a reliable estimation of the magnetic field spectra for both components and are thus dependent on an accurate separation.

From the GIC viewpoint, the importance of the field separation is not in the practical modeling of GIC or in understanding the basic ionospheric dynamics. The importance comes forward in the usage of the separated fields in determining the ground conductivity structure, which is naturally of a great importance for GIC studies. The separation of the field is also required in the studies where the GIC modeling is made in detail far beyond the scope of the work presented here. This type of future work is described in Chapter 4.

The separation of the magnetic disturbance field into external and internal parts is carried out here by utilizing the SECS method. Similarly to the equivalent current determination, there are traditional methods which are used, namely the Gauss-Schmidt (Chapman and Bartels, 1940), the spherical cap harmonics (Haines, 1985), the Fourier (Weaver, 1964; Mersmann et al., 1979) and the spatial (Siebert and Kertz, 1957) method<sup>1</sup>. The SECS method has significant advantages over these methods. The advantages are basically the computational efficiency and the possibility to make local choices for the spatial resolution of the determined fields. The idea of the SECS separation is to establish two layers of divergence-free elementary systems, one above the surface of the Earth ( $r = R_I > R_e$ ) and another below it ( $r = R_G < R_e$ ). Using the notations of Eq. (2.18), the magnetic field at the surface of the Earth can be expressed as

$$\mathbf{B}(\vartheta, \varphi) = \sum_{j=1}^M I_j \mathbf{T}_{df}^j(\vartheta, \varphi) + \sum_{k=1}^S \tilde{I}_k \tilde{\mathbf{T}}_{df}^k(\vartheta, \varphi) \quad (2.27)$$

where tilde denotes the scaling factors and geometric parts of the fields

---

<sup>1</sup>The spatial and the Fourier method are mathematically equivalent via convolution theorem

corresponding to the internal layer at  $r = R_G$ . Now for a discrete set of  $N$  measurements of the ground magnetic field at locations  $(\vartheta_i, \varphi_i)$  we obtain a set of equations similar to (2.19). The equations can be solved as before in the least squares sense using SVD. Once  $\mathbf{I}$  and  $\tilde{\mathbf{I}}$  are known, the separated field components can be computed from Eq. (2.27). Note that again any ground magnetic field variation can be expressed in terms of Eq. (2.27).

## 2.2 Computation of the ground geoelectric field

Before going into details, let us review some of the basic properties of electromagnetic fields of geomagnetic origin. The mathematics will be discussed in the planar geometry where the standard choice of the coordinate system in geophysics is utilized ( $x$  north,  $y$  east,  $z$  downward, origin at the surface of the Earth). Neglecting the Earth's curvature is acceptable for local studies (dimensions less than 1000 km), a requirement that is perfectly fulfilled in this work. The fundamental properties of the fields are expressed by Maxwell's equations and Ohm's law:

$$\nabla \cdot \mathbf{E} = \rho/\epsilon \quad (2.28)$$

$$\nabla \cdot \mathbf{B} = 0 \quad (2.29)$$

$$\nabla \times \mathbf{E} = -\frac{\partial \mathbf{B}}{\partial t} \quad (2.30)$$

$$\nabla \times \mathbf{B} = \mu_0 \mathbf{j} + \mu_0 \epsilon \frac{\partial \mathbf{E}}{\partial t} \quad (2.31)$$

$$\mathbf{j} = \sigma \mathbf{E} \quad (2.32)$$

where the standard notation is used (see page vii). The media are assumed to be nonmagnetic, i.e. the magnetic permeability of vacuum  $\mu_0 = 4\pi \cdot 10^{-7}$  H/m is used. This is a valid and commonly used assumption in all geomagnetic induction studies.

Taking curl of Eq. (2.30) and using Eqs. (2.31) - (2.32) we obtain

$$\nabla^2 \mathbf{E} = \nabla(\nabla \cdot \mathbf{E}) + \mu_0 \sigma \frac{\partial \mathbf{E}}{\partial t} + \mu_0 \epsilon \frac{\partial^2 \mathbf{E}}{\partial t^2} \quad (2.33)$$

Following the treatment by Weaver (1994), we define a dimensionless parameter  $t' = t/T$  where  $T$  is the characteristic time of the phenomena under investigation. Substituting  $t'$  into Eq. (2.33), we obtain

$$\nabla^2 \mathbf{E} = \nabla(\nabla \cdot \mathbf{E}) + \kappa_1 \frac{\partial \mathbf{E}}{\partial t'} + \kappa_2 \frac{\partial^2 \mathbf{E}}{\partial t'^2} \quad (2.34)$$

where  $\kappa_1 = \mu_0\sigma/T$  and  $\kappa_2 = \mu_0\epsilon/T^2$ . When the smallest time scales of interest (1 s) and the lowest estimate for a possible ground conductivity (order of  $10^{-5}$  S/m) and the vacuum value for the permittivity  $\epsilon$  are chosen we find that  $\kappa_1/\kappa_2 = \sigma T/\epsilon_0$  is of the order of  $10^8$ , i.e.  $\kappa_1 \gg \kappa_2$ . Consequently, the last term in Eq. (2.34) can be neglected. This is the so-called quasi-stationary approximation which is generally valid for all geomagnetic induction applications. The quasi-static approximation is equivalent to neglecting the last term in Eq. (2.31), i.e. the displacement current. By applying the approximation, we see from Eq. (2.31) that  $\nabla \cdot \mathbf{j} = 0$ , i.e. the current in the Earth is divergence-free. The divergence-free condition applied to Eq. (2.32) gives

$$(\nabla\sigma) \cdot \mathbf{E} + \sigma\nabla \cdot \mathbf{E} = 0 \quad (2.35)$$

By solving  $\nabla \cdot \mathbf{E}$  from this expression and substituting into the quasi-stationary version of Eq. (2.33) we obtain

$$\nabla^2\mathbf{E} = -\nabla((\nabla\sigma) \cdot \mathbf{E}/\sigma) + \mu_0\sigma\frac{\partial\mathbf{E}}{\partial t} \quad (2.36)$$

A significant simplification of Eq. (2.36) is obtained if gradients of the conductivity can be neglected. A common way to do this is to use a block model of the Earth where the conductivity is uniform within each block. This is valid in regions where geological structures rather than temperature gradients cause variations of the conductivity. Usually in GIC studies, the Earth conductivity structure is assumed to be locally either one-dimensional (conductivity blocks just in the  $z$  direction), i.e. layered, or completely uniform. These are the assumptions used also in this work. If  $\nabla\sigma = 0$  Eq. (2.36) takes the form

$$\nabla^2\mathbf{E} = \mu_0\sigma\frac{\partial\mathbf{E}}{\partial t} \quad (2.37)$$

which is the vector diffusion equation for the electric field. Noteworthy is that due to the neglected displacement currents Eq. (2.37) describes a field that is behaving diffusively in the medium rather than propagating as an electromagnetic wave. Furthermore, it is an easy task to show that also the magnetic field satisfies the diffusion equation in a uniform conductor

$$\nabla^2\mathbf{B} = \mu_0\sigma\frac{\partial\mathbf{B}}{\partial t} \quad (2.38)$$

The diffusion equations with boundary conditions for the electromagnetic fields form the basis for the standard treatment of the geomagnetic induction

problem (see e.g., Weaver, 1994).

It is also worth noting that due to the very small conductivity of the air (order of  $10^{-14}$  S/m), there is in practice no *galvanic* connection between the Earth and ionospheric or magnetospheric current sources. It follows, that the electromagnetic field in the Earth is of *inductive* origin. Furthermore, if there are no horizontal variations in the Earth's conductivity, the electric field inside the Earth is always horizontal, i.e. the vertical component  $E_z$  is always zero. This is seen by using the boundary condition of the current density

$$\sigma_1 \mathbf{E}_1 \cdot \mathbf{n} = \sigma_2 \mathbf{E}_2 \cdot \mathbf{n} \quad (2.39)$$

where  $\mathbf{n}$  is the unit vector normal to the boundary. This follows from the  $\nabla \cdot \mathbf{j} = 0$  condition. If the conductivity of the air is taken to be zero, it follows from (2.39) that the vertical component of electric field right below the surface must be zero. If also at the bottom layer, or at  $z \rightarrow \infty$ , the vertical field is zero, it follows that the only solution of Eq. (2.37) for the vertical component is  $E_z = 0$  inside the Earth, i.e. the electric field is horizontal.

### 2.2.1 Computation via surface magnetic field

From the viewpoint of the study at hand, it is of great interest to know the relation between the variations of the ground magnetic field and the horizontal geoelectric field  $E_{(x,y)}(z=0)$  driving GIC. Contrary to the geoelectric field measurements, good quality ground magnetic field data are available from numerous stations distributed throughout the world, and long time series are available. Thus, it is clear that the ground geomagnetic field is a key quantity for the GIC modeling.

Let us start from Eq. (2.37). Express  $\mathbf{B} = (B_x, B_y, B_z)$  and  $\mathbf{E} = (E_x, E_y, E_z)$  as Fourier integrals

$$\mathbf{B}(x, y, z, t) = \frac{1}{(2\pi)^{3/2}} \int \int \int_{-\infty}^{\infty} \mathbf{b}(\alpha, \beta, z, \omega) e^{i(\alpha x + \beta y + \omega t)} d\alpha d\beta d\omega \quad (2.40)$$

$$\mathbf{E}(x, y, z, t) = \frac{1}{(2\pi)^{3/2}} \int \int \int_{-\infty}^{\infty} \mathbf{e}(\alpha, \beta, z, \omega) e^{i(\alpha x + \beta y + \omega t)} d\alpha d\beta d\omega \quad (2.41)$$

where  $\mathbf{b} = (b_x, b_y, b_z)$  and  $\mathbf{e} = (e_x, e_y, e_z)$ . Then Eq. (2.37) reduces to

$$\frac{\partial^2 \mathbf{e}}{\partial z^2} - \gamma^2 \mathbf{e} = 0 \quad (2.42)$$



where  $\gamma^2 = \alpha^2 + \beta^2 + i\omega\mu_0\sigma$ . The solution of Eq. (2.42) for horizontal components can be expressed as

$$e_{(x,y)}(z) = c_{(x,y)}e^{\gamma z} + d_{(x,y)}e^{-\gamma z} \quad (2.43)$$

where  $c$  and  $d$  are complex values and we choose  $Re(\gamma) > 0$ .<sup>2</sup> From Eq. (2.30), using Eqs. (2.40) and (2.41) and utilizing the fact that  $E_z = 0$  inside the Earth, we obtain

$$\frac{\partial e_y}{\partial z} = i\omega b_x \quad (2.44)$$

$$\frac{\partial e_x}{\partial z} = -i\omega b_y \quad (2.45)$$

$$\beta e_x - \alpha e_y = \omega b_z \quad (2.46)$$

The task is to find the relation between the horizontal components of the magnetic field and the geoelectric field at the surface of the Earth. Let us define the spectral impedance as

$$Z = \mu_0 \frac{e_x}{b_y} = -\mu_0 \frac{e_y}{b_x} \quad (2.47)$$

Where the last equality can be verified using conditions  $[\nabla \times \mathbf{B}]_z = 0$  and  $\nabla_h \cdot \mathbf{E} = 0$  which follow from the  $E_z = 0$  condition. Using Eq. (2.43) and Relations (2.44) and (2.45) we obtain

$$Z = -\frac{i\omega\mu_0}{\gamma} \frac{c_{(x,y)}e^{\gamma z} + d_{(x,y)}e^{-\gamma z}}{c_{(x,y)}e^{\gamma z} - d_{(x,y)}e^{-\gamma z}} \quad (2.48)$$

which can be rewritten as

$$Z = -\frac{i\omega\mu_0}{\gamma} \coth(\gamma z + s) \quad (2.49)$$

where  $s = \ln(\sqrt{c_{(x,y)}/d_{(x,y)}})$ .

Eq. (2.49) is valid for a uniform conductor. Next we consider a layered Earth structure. Now with  $\gamma^2 \rightarrow \gamma_n^2 = \alpha^2 + \beta^2 + i\omega\mu_0\sigma_n$  and  $s \rightarrow s_n$  at layer  $z_n \leq z \leq z_{n+1}$  we can write (2.49) at the bottom of the layer ( $z = z_{n+1}$ ) as

$$Z(z_{n+1}) = -\frac{i\omega\mu_0}{\gamma_n} \coth(\gamma_n z_{n+1} + s_n) \quad (2.50)$$

---

<sup>2</sup>The same convention is applied henceforth for all square roots of complex numbers

and at the top of the layer ( $z = z_n$ ) as

$$Z(z_n) = -\frac{i\omega\mu_0}{\gamma_n} \coth(\gamma_n z_n + s_n) \quad (2.51)$$

By eliminating  $s_n$  from these expressions we obtain a recursive formula

$$Z(z_n) = \frac{i\omega\mu_0}{\gamma_n} \coth(\gamma_n d_n + \coth^{-1}(\frac{\gamma_n}{i\omega\mu_0} Z(z_{n+1}))) \quad (2.52)$$

where  $d_n = z_{n+1} - z_n$ . Eq. (2.52) is known as *Lipskaya formula* (Berdichevsky and Zhdanov, 1984, p. 53) and it determines the spectral impedance at the top of the  $n$ th layer in terms of the impedance at the bottom of the layer. In general the impedance is dependent on the frequency and also on the wavenumbers  $\alpha$  and  $\beta$ . To obtain the surface impedance  $Z^0$ , one just sets  $n = 1$  in Eq. (2.52) and computes the impedance values recursively starting from the bottom of the modeled Earth structure.

Let us then investigate in greater detail Relation (2.47). First we move back into the spatio-temporal domain. Using (2.41) we obtain

$$\begin{aligned} E_{(x,y)}^0(x, y, t) &= \frac{1}{(2\pi)^{3/2}} \int \int \int_{-\infty}^{\infty} e_{(x,y)}^0 e^{i(\alpha x + \beta y + \omega t)} d\alpha d\beta d\omega \\ &= \pm \frac{1}{(2\pi)^{3/2} \mu_0} \int \int \int_{-\infty}^{\infty} Z^0 b_{(y,x)}^0 e^{i(\alpha x + \beta y + \omega t)} d\alpha d\beta d\omega \end{aligned} \quad (2.53)$$

where the subscript 0 denotes the corresponding quantities at the surface of the Earth ( $z = 0$ ). Concentrating here just on the  $x$ -component (the  $y$ -component is handled identically) and applying the convolution theorem to Eq. (2.53), we obtain

$$E_x^0(x, y, t) = \frac{1}{(2\pi)^{3/2} \mu_0} \int \int \int_{-\infty}^{\infty} G(x', y', t')^0 B_y^0(x - x', y - y', t - t') dx' dy' dt' \quad (2.54)$$

where the kernel of the integral is defined as

$$G(x', y', t')^0 = \frac{1}{(2\pi)^{3/2}} \int \int \int_{-\infty}^{\infty} Z^0 e^{i(\alpha x' + \beta y' + \omega t')} d\alpha d\beta d\omega \quad (2.55)$$

Consequently, if we are able to evaluate the integral in (2.55), we can transform the horizontal magnetic field measured at the Earth's surface into the horizontal geoelectric field via Eq. (2.54). However, one usually does not

know the magnetic field from very large (infinite) area and over very long time intervals and thus some approximations are needed for practical applications. Let us investigate, in the fashion of Dmitriev and Berdichevsky (1979), the basic properties of  $G(x', y', t')^0$  in the case of a uniform ground conductivity structure. By setting  $d_n$  equal to infinite in Eq. (2.52), we obtain

$$G(x', y', t')^0 = \frac{i\mu_0}{(2\pi)^{3/2}} \int \int \int_{-\infty}^{\infty} \frac{\omega}{\gamma_n} e^{i(\alpha x' + \beta y' + \omega t')} d\alpha d\beta d\omega \quad (2.56)$$

The spatial part of Eq. (2.56) can be transformed into a Hankel integral (e.g., Arfken and Weber, 1995, p. 849)

$$G(r', t')^0 = \frac{i\mu_0}{\sqrt{2\pi}} \int_{-\infty}^{\infty} \int_0^{\infty} \frac{\omega}{\sqrt{\rho^2 + k^2}} \rho J_0(r' \rho) e^{i\omega t'} d\rho d\omega \quad (2.57)$$

where  $r' = \sqrt{x'^2 + y'^2}$ ,  $\rho = \sqrt{\alpha^2 + \beta^2}$ ,  $k^2 = i\omega\mu\sigma$  and  $J_0$  is the zeroth order Bessel function. The integration with respect to  $\rho$  gives (Gradshteyn and Ryzhik, 1965, formula 6.554.1)

$$G(r', t')^0 = \frac{i\mu_0}{\sqrt{2\pi}} \int_{-\infty}^{\infty} \frac{\omega e^{-kr'}}{r'} e^{i\omega t'} d\omega \quad (2.58)$$

Before proceeding it is noted that the quasi-static approximation has been used, i.e.  $\sigma T/\epsilon$  was assumed to be large. This is strictly valid for all temporal variations only if  $\sigma/\epsilon$  approaches infinity. However, the highest frequencies of the relevant geomagnetic variations observable on the ground rarely exceed 1 Hz and thus in practice the quasi-static approximation holds for all temporal variations of geomagnetic origin (see e.g., Keller and Frischknecht, 1970, p. 200). We seek for a pragmatic approach and thus we assume that the contribution from the frequencies above the validity of the quasi-static approximation to the  $b_{(x,y)}^0$  term of Eq. (2.53) are negligible. Consequently, it is reasonable to carry out the integration in Eq. (2.58) from  $-\infty$  to  $\infty$  since the frequencies for which the approximation is not valid, do not contribute to the final geoelectric field (see also discussion by Pirjola, 1982, p. 20-25). Let us then investigate the causality. By making a substitution  $\sqrt{\omega} = \kappa$ , the integral (including only terms contributing to the integral) appearing in Eq. (2.58) can be written as

$$2 \int_0^{\infty} \kappa^3 e^{-c\kappa + i\kappa^2 t'} d\kappa - 2 \int_0^{\infty} \kappa^3 e^{ic\kappa - i\kappa^2 t'} d\kappa \quad (2.59)$$

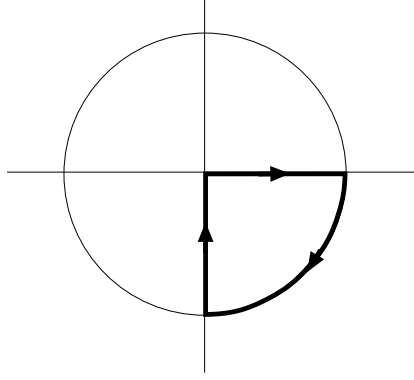


Figure 2.3: Contour in the complex plane along which the integration is carried out to obtain Relation (2.60).

where  $c$  is a complex value. Now by assuming that  $t' < 0$  and by integrating the first term of Eq. (2.59) in a lower complex half plane along the contour shown in Fig. 2.3, we obtain the relation

$$\int_0^{\infty} \kappa^3 e^{-c\kappa + i\kappa^2 t'} d\kappa = \int_0^{\infty} \kappa^3 e^{i c\kappa - i\kappa^2 t'} d\kappa \quad (2.60)$$

Accordingly, it is obvious that the integral in Eq. (2.58) vanishes for  $t' < 0$  and the causality is preserved: The future does not affect the history. For  $t' > 0$  Eq. (2.58) can be integrated using the parabolic cylinder function to yield (Gradshteyn and Ryzhik, 1965, see formulas 3.462.1, 9.248.2 and 9.251)

$$G(r', t')^0 = \frac{1}{2^{5/2}} \frac{\mu_0}{r' t'^2} \left( \frac{\mu_0 \sigma r'^2}{t'} \right)^{3/2} \left( 1 - \frac{6t'}{\mu_0 \sigma r'^2} \right) e^{-\frac{\mu_0 \sigma r'^2}{4t'}} H(t') \quad (2.61)$$

where  $H(t')$  is the Heaviside unit step function.

There are a number of interesting features in Relation (2.61). Firstly, as can be seen from the  $t'^{7/2}$  term in the denominator,  $G(r', t')^0$  is temporally relatively local. From the term  $-\frac{\mu_0 \sigma r'^2}{4t'}$  in the exponential, it is seen that  $G(r', t')^0$  is also spatially local and due to the  $r'$  dependence, axially symmetric. Fig. (2.4) shows  $-G(r', t')^0$  as a function of time  $t'$  and radial distance  $r'$ . In the figure,  $\sigma = 10^{-2}$  S/m which represents the *effective* conductivity of the southern part of Finland (Viljanen, 1998; Paper II), was used and the computation is started from  $t' = 10$  s to avoid the singularity

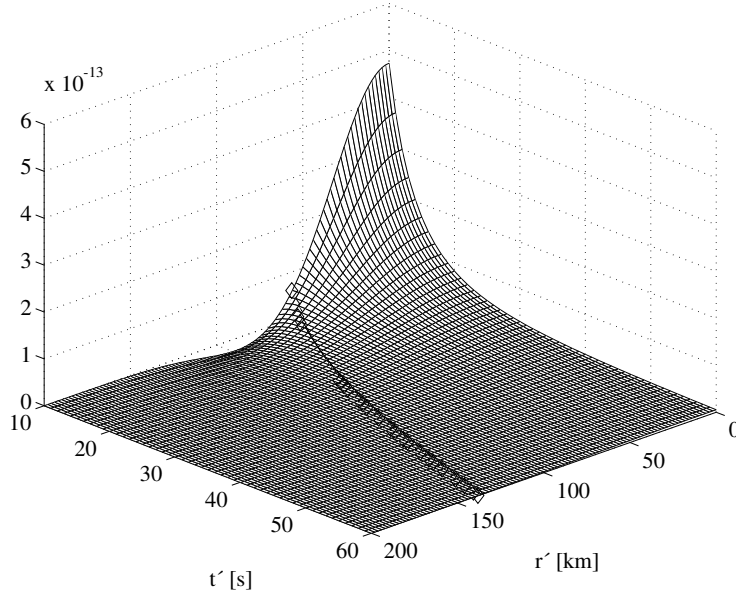


Figure 2.4: Temporal and spatial behavior of  $-G(r', t')^0$  in Eq. (2.61).  $\sigma = 10^{-2}$  S/m has been used in computing the values. The diamonds denote the values  $r'_s = \sqrt{\frac{4t'}{\mu_0\sigma}}$ .

at the origin. As it is seen from the figure, the main contribution to  $G(r', t')^0$  comes from the vicinity of the origin. The decay to  $1/e$  is obtained at the radius  $r'_s = \sqrt{\frac{4t'}{\mu_0\sigma}}$ . With the chosen Earth parameters this is less than 150 km for  $t' = 60$  s. Thus it is obvious that for obtaining the effective values for  $E_x^0(x, y, t)$  in Eq. (2.54), we do not need information about the ground magnetic field variations from distances of several hundreds of kilometers. Furthermore, if we may assume that the spatial magnetic field variations within the effective radius of  $G(r', t')^0$  are linear, we need only one measurement point of the magnetic field to compute the local effective geoelectric field  $E_x^0(x, y, t)$ . This is due to axial symmetry of  $G(r', t')^0$  and is easily seen by substituting

$$\begin{aligned} B_y^0(x - x', y - y', t - t') &= B_y^0(x, y, t - t') + ax' + by' \\ &= B_y^0(x, y, t - t') + ar' \cos(\phi') + br' \sin(\phi') \end{aligned} \quad (2.62)$$

where  $a$  and  $b$  are just some constants and where the transformation to

cylindrical coordinates has been made. In cylindrical coordinates Eq. (2.54) becomes

$$\begin{aligned} E_x^0(x, y, t) &= \frac{1}{(2\pi)^{3/2}\mu_0} \int_0^\infty \int_0^{2\pi} \int_0^\infty G(r', t')^0 [B_y^0(x, y, t - t') + \\ &\quad ar' \cos(\phi') + br' \sin(\phi')] r' dr' d\phi' dt' \\ &= \frac{1}{\sqrt{2\pi}\mu_0} \int_0^\infty \int_0^\infty G(r', t')^0 B_y^0(x, y, t - t') r' dr' dt' \end{aligned} \quad (2.63)$$

where the  $r'$  dependence is found only in  $G(r', t')^0$  and thus the magnetic field is needed only at point  $(x, y)$ . Let us now assume spatially linear magnetic field variations and substitute (2.61) to (2.63). From this, the  $r'$  dependence is eliminated by integration (Gradshteyn and Ryzhik, 1965, formula 3.461.3) and we obtain

$$E_x^0(x, y, t) = -\frac{1}{2\sqrt{\pi}\mu_0\sigma} \int_0^\infty \frac{B_y^0(x, y, t - t')}{t'^{3/2}} dt' \quad (2.64)$$

This can be further modified by integrating by parts. We get

$$E_x^0(x, y, t) = -\frac{1}{\sqrt{\pi}\mu_0\sigma} \int_0^\infty \frac{g_y^0(x, y, t - t')}{\sqrt{t'}} dt' \quad (2.65)$$

where  $g_y^0 = dB_y^0/dt'$ . And finally, this can be written as

$$E_x^0(x, y, t) = \frac{1}{\sqrt{\pi}\mu_0\sigma} \int_{-\infty}^t \frac{g_y^0(x, y, t')}{\sqrt{t - t'}} dt' \quad (2.66)$$

Identically, for the  $E_y$ -component we obtain

$$E_y^0(x, y, t) = -\frac{1}{\sqrt{\pi}\mu_0\sigma} \int_{-\infty}^t \frac{g_x^0(x, y, t')}{\sqrt{t - t'}} dt' \quad (2.67)$$

Well known Relations (2.66)-(2.67) are identical to those that would have been obtained by assuming the source field to be a downward propagating plane wave, the assumption forming the basis of the magnetotelluric sounding method (Cagniard, 1953). However, as was seen above, the plane wave requirement can be relaxed to assumptions about the locally ( $\sim 100$  km) linear behavior of the surface magnetic variations. This is a result that simplifies the practical GIC modeling significantly. To estimate the local geoelectric field behavior we need geomagnetic recordings only from one single point.

Above the uniform ground conductivity was employed. For layered Earth conductivity structures the situation becomes more difficult. Anyhow, the main conclusions above hold for typical conductivity structures (Dmitriev and Berdichevsky, 1979). An approach for modeling a multilayered Earth is to use Eq. (2.52) with  $\alpha$  and  $\beta$  equal to zero (plane wave) and computing the surface impedance using the known conductivities of the layers. The computation of the electric field is made in the frequency domain via Eqs. (2.47) and the time domain field is obtained by Fourier transforms. However, although the multilayered approach is in principle more exact, it has been seen in numerous investigations that in practice Eqs. (2.66)-(2.67), applied with some effective conductivity estimate exhibiting the average behavior of the fields with relevant periods, are able to give the surface geoelectric field with an accuracy sufficient for GIC modeling (e.g., Viljanen and Pirjola, 1989; Viljanen, 1998; Paper I). The main requirement is that the magnetic data used is from the vicinity of the GIC-modeling region. Also, Relations (2.66)-(2.67) are directly applicable to real-time computations.

Worth noting here is that Relations (2.66)-(2.67) suggest that there is a close connection between the time derivative of the horizontal magnetic field and the horizontal surface geoelectric field, i.e.  $dB_{x,y}/dt \sim E_{y,x}$ . Consequently, the time derivative of the horizontal magnetic field is a good indicator for GIC activity (Viljanen et al., 2001). This feature will be utilized in Chapter 3.

### 2.2.2 Computation using a known ionospheric current system

If, instead of ground magnetic field variations, the ionospheric current system is known, another pragmatic approach can be used for GIC-related geoelectric field computations. The method is based on the complex image representation of the ground induction contribution and it simplifies the equations for the total electromagnetic field at the surface of the Earth significantly. The fundamental idea behind the complex image method (CIM) was presented by Wait and Spies (1969) and is reviewed below.

Let us again assume a homogeneous Earth with the conductivity  $\sigma$ , zero air conductivity and a horizontal ionospheric source current (see Fig. 2.5). Any three-dimensional ionospheric source current can be equivalently represented by a horizontal current distribution, as was shown in Section 2.1. Horizontal ionospheric currents do not produce a vertical electric field, thus also the primary component, i.e. the field in the absence of the conducting Earth,  $E_z^p = 0$ . The  $x$ -component of the electric field in the region between

the surface of the Earth and ionosphere ( $-h < z \leq 0$ ) and in the Earth ( $z \geq 0$ ) can be expressed using Eq. (2.43) with the boundary condition  $e_x^1(\infty) = 0$

$$e_x^0(z) = c_x^0 e^{\gamma_0 z} + e_x^p(0) e^{-\gamma_0 z}, \quad -h < z \leq 0 \quad (2.68)$$

$$e_x^1(z) = d_x^1 e^{-\gamma_1 z}, \quad z \geq 0 \quad (2.69)$$

where  $e_x^p(0)$  is the spectrum  $(\alpha, \beta, \omega)$  of the  $x$ -component of the primary electric field at the surface. The continuity of  $b_y$  and  $e_x$  across the boundary  $z = 0$  with Relation (2.45) implies

$$c_x^0 + e_x^p(0) = d_x^1 \quad (2.70)$$

$$\gamma_0 c_x^0 - \gamma_0 e_x^p(0) = -\gamma_1 d_x^1 \quad (2.71)$$

from which  $c_x^0$  can be solved and Eq. (2.68) takes the form

$$e_x^0(z) = \frac{\gamma_0 - \gamma_1}{\gamma_0 + \gamma_1} e_x^p(0) e^{\gamma_0 z} + e_x^p(0) e^{-\gamma_0 z} \quad (2.72)$$

where the first term on the right-hand side represents the secondary field arising from induction in the Earth (denoted below by  $e_x^{0,ind}(z)$ ). Let us take a closer look at this term. We multiply the term by  $e^{\gamma_0 2p} e^{-\gamma_0 2p}$ , i.e. by one.  $p$  is so far an arbitrary parameter and is not to be confused with the primary component of the electric field. One obtains

$$e_x^{0,ind}(z) = \frac{\gamma_0 - \gamma_1}{\gamma_0 + \gamma_1} e^{\gamma_0 2p} e_x^p(0) e^{\gamma_0(z-2p)} = K(\eta) e_x^p(0) e^{\gamma_0(z-2p)} \quad (2.73)$$

where we have defined  $\alpha^2 + \beta^2 = \eta^2$ . Accordingly,  $\gamma_0 = \eta$  and  $\gamma_1 = \sqrt{\eta^2 + i\omega\mu_0\sigma}$ . Next we define

$$p = \lim_{\eta \rightarrow 0} \frac{Z^0}{i\omega\mu_0} \quad (2.74)$$

where  $Z^0(\eta = 0)$  is the surface impedance, given by Eq. (2.52) with  $n = 1$ , for a uniform inducing field (plane wave). Using the chosen definitions we expand  $K(\eta)$  around  $\eta = 0$

$$K(\eta) = \sum_{n=0}^{\infty} \frac{\eta^n}{n!} K^{(n)}(0) = -1 - \frac{\eta^3}{3(i\omega\mu_0\sigma)^{(3/2)}} + \mathcal{O}(\eta^5) \quad (2.75)$$



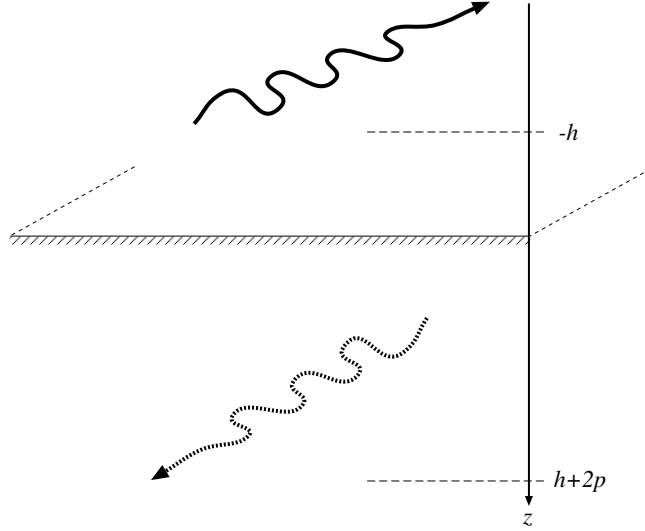


Figure 2.5: Ionospheric horizontal source current located at  $z = -h$  and its complex image located at  $z = h + 2p$  representing the induction part of the electromagnetic field for  $-h < z \leq 0$ .

Remarkable is that the first and the second order terms of Eq. (2.75) vanish. It follows that (2.73) can be approximated by

$$e_x^{0,ind}(z) \approx -e_x^p(0)e^{\gamma_0(z-2p)} \quad (2.76)$$

if  $|\left(\frac{\eta}{\sqrt{i\omega\mu_0\sigma}}\right)|^3 \ll 1$ . The denominator is equal to  $1/p$ , where  $p$  is identifiable as a complex skin depth. It is clear that the approximation becomes worse when the complex skin depth increases, i.e. wave frequency or conductivity of the Earth decreases or if the spatial wavelength of the horizontal field variations decreases.

The  $y$ -component of the electric field is treated identically to the  $x$ -component, and the total electric ( $e_z^0 = 0$ ) field can thus be written as

$$\mathbf{e}^0(z) \approx -\mathbf{e}^p(0)e^{\gamma_0(z-2p)} + \mathbf{e}^p(0)e^{-\gamma_0 z} \quad (2.77)$$

The secondary field tends to diminish the total geoelectric field. This is expected since  $\mathbf{e}^0(0) \rightarrow 0$  for  $\sigma \rightarrow \infty$ .

A corresponding treatment for the magnetic field is given via Eqs. (2.44)-(2.46). By substituting (2.77) into (2.44) and (2.45) one obtains for horizontal magnetic field components

$$b_{(x,y)}^0(z) \approx b_{(x,y)}^p(0)e^{\gamma_0(z-2p)} + b_{(x,y)}^p(0)e^{-\gamma_0 z} \quad (2.78)$$

where  $b_{(x,y)}^p(0)$  are the spectrum  $(\alpha, \beta, \omega)$  of the horizontal components of the primary magnetic field at the surface of the Earth. The vertical magnetic field component is treated similarly by substituting (2.77) into (2.46). One obtains

$$b_z^0(z) \approx -b_z^p(0)e^{\gamma_0(z-2p)} + b_z^p(0)e^{-\gamma_0 z} \quad (2.79)$$

where again the secondary field tends to diminish the total vertical field. This is also expected since  $b_z^0(0) \rightarrow 0$  for  $\sigma \rightarrow \infty$ .

Let us next write the functions in Eqs. (2.77)-(2.79) as

$$f(0)e^{\gamma_0(z-2p)} = g(\alpha, \beta, -(z-2p)) \quad (2.80)$$

Then by Fourier-inverting these with respect to  $\alpha$  and  $\beta$  one obtains

$$\mathbf{E}^0(x, y, z) \approx -\mathbf{E}^p(x, y, 2p-z) + \mathbf{E}^p(x, y, z) \quad (2.81)$$

$$\mathbf{B}^0(x, y, z) \approx \mathbf{B}_H^p(x, y, 2p-z) - \mathbf{B}_z^p(x, y, 2p-z) + \mathbf{B}^p(x, y, z) \quad (2.82)$$

where  $H$  denotes the horizontal component. Eqs. (2.81) and (2.82) can be interpreted as follows: If the primary ionospheric current source is located at  $z = -h$ , then the field due to induction in the Earth is represented by an image current of the primary source placed at the complex depth  $z = h + 2p$  (see Fig. 2.5). Note that Expressions (2.81) and (2.82) are valid in the frequency domain and the location of the complex image depends on the frequency. Simple Relations (2.74), (2.81) and (2.82) permit an easy and fast calculation of the total electromagnetic field at  $-h < z \leq 0$  if the primary electromagnetic field caused by the source is known.

Although the treatment above was given for a homogeneous Earth, it can be shown, by using a completely analogous approach, that CIM also works with general layered Earth conductivity structures (Thomson and Weaver, 1975). Furthermore, it has been shown that CIM is applicable to numerous different types of sources and that the accuracy of the method is perfectly sufficient for GIC-related computations (Thomson and Weaver, 1975; Boteler and Pirjola, 1998; Pirjola and Viljanen, 1998).

It is worth to note that CIM can be directly combined with the ionospheric elementary sources presented in Section 2.1. As shown in Paper III, the realization of the combination is quite straightforward: First the elementary current system method is applied to the measurements of the

ground magnetic field, giving a set of scaling factors  $\mathbf{I}$  of the divergence-free elementary systems. By knowing the ground conductivity structure and the electromagnetic field produced by a harmonically varying horizontal current system on the right-hand side of Fig. 2.2, we are able to apply CIM Eqs. (2.81) and (2.82) and compute the total electromagnetic field at the surface. This approach permits the computation of the induced fields for different layered Earth conductivity structures using true ionospheric sources, instead of idealized models. For an explicit expression of the electromagnetic field produced by a divergence-free elementary system see Paper III. Note that the expressions are derived in the Cartesian geometry. However, as shown by Viljanen et al. (2003), the usage of the scaling factors derived in the spherical geometry in the electromagnetic field expressions of the Cartesian system does not introduce any errors of practical significance.

## 2.3 Computation of geomagnetically induced currents

### 2.3.1 Discretely grounded systems

When the surface geoelectric field is known, we are ready to carry out the actual GIC calculation. The problem can be divided into two types of approaches used for different systems. The first type belongs to the discretely grounded systems, like power transmission systems, and the second to continuously grounded systems, for example buried pipelines. Note that buried pipelines, though coated with insulating material (conductivities of the order of  $10^{-8}$  S/m), are in galvanic connection to the Earth. Common for both approaches is that they are essentially direct-current (dc) solutions. This means that each time instant can be treated separately taking only into account the electric field at the particular time instant and GIC are solved using the dc parameters of the systems under investigation. The dc approach is rigorously validated, for the first time, below.

Let us first look how discretely grounded systems are handled (Lehtinen and Pirjola, 1985; Pirjola and Lehtinen, 1985). Although we discuss power transmission lines below, the same treatment is valid for all discretely grounded systems. The set-up of the power transmission model is shown in Fig 2.6. We start by integrating Faraday's law, Eq. (2.30), over the surface  $A$  defined by  $i, j, j'$  and  $i'$

$$\oint \mathbf{E} \cdot d\mathbf{s} = - \int_A \frac{\partial \mathbf{B}}{\partial t} \cdot d\mathbf{a} \quad (2.83)$$

where  $\mathbf{a}$  is a unit vector perpendicular to the surface  $A$ . The left-hand side of Eq. (2.83) becomes

$$Z_{ij}^{int} I_{ij}^n + \int_{j'}^{i'} \mathbf{E} \cdot d\mathbf{s} \quad (2.84)$$

where  $Z_{ij}^{int}$  is the total internal impedance of the transmission line between points  $i$  and  $j$ ,  $I_{ij}^n$  is the corresponding electric current flowing in the line  $n$ . The total field  $\mathbf{E}$  in Eq. (2.84) is the sum of different sources, i.e.  $\mathbf{E} = \mathbf{E}^0 + \mathbf{E}^n + \mathbf{E}^c$ , where  $\mathbf{E}^0$  is the surface electric field in the absence of the power transmission line,  $\mathbf{E}^n$  is the secondary electric field produced by the varying currents in the transmission line and  $\mathbf{E}^c$  is the electric field produced by the currents injected from the transmission line to the Earth. The  $\mathbf{E}^c$  related term in Eq. (2.84) is just the potential difference between the injection points  $j'$  and  $i'$  and can be expressed as

$$\int_{j'}^{i'} \mathbf{E}^c \cdot d\mathbf{s} = U_j^c - U_i^c \quad (2.85)$$

where the potentials  $U_{i,j}^c$  can be expressed as

$$U_j^c = \sum_{i=1}^m Z_{ji}^e I_i^e \quad (2.86)$$

where  $Z_{ji}^e$  is the earthing impedance matrix and  $I_i^e$  are the earthing currents injected to the Earth through  $i$  (and  $i'$ ). The earthing impedance matrix  $Z_{ji}^e$  is diagonal if the earthing points are so distant from each other that no electromagnetic coupling exists between them. This is usually the case in practice.

The  $\mathbf{E}^n$  term in Eq. (2.84) is, for simplicity, searched for by using the complex image approximation for an infinite line current above homogeneous Earth of conductivity  $\sigma$ . The field produced at the surface by the harmonic ( $e^{i\omega t}$ ) primary source at height  $z = -h$  ( $x = 0$ , positive current flow  $I$  along the  $y$  axis) and its complex image at depth  $(h + 2p)$  can be expressed as (e.g., Boteler and Pirjola, 1998)

$$E_y = -\frac{i\omega\mu_0 I}{2\pi} \ln \left( \frac{\sqrt{(h+2p)^2 + x^2}}{\sqrt{h^2 + x^2}} \right) \quad (2.87)$$

where for the uniform Earth  $p = 1/\sqrt{i\omega\mu_0\sigma}$ . Thus,  $\mathbf{E}^n$  right below the transmission line ( $x = 0$ ) caused by the current  $I_{ij}^n$  can be written as

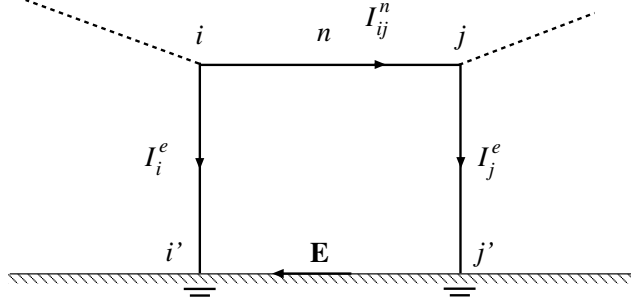


Figure 2.6: Model of the power transmission system. In reality wire  $i \rightarrow j$  is composed of three wires related to different phases of the transmitted electricity and points  $i$  and  $j$  are the neutral points of the power transformers. The total electric field  $\mathbf{E}$  acts as a driver of the system.

$$E_{j'i'}^n = \frac{I_{ij}^n i \omega \mu_0}{2\pi} \ln \left( \frac{h + 2p}{h} \right) \quad (2.88)$$

Eq. (2.88) will allow us to estimate the strength of the inductive coupling between the transmission line and the Earth.

By defining

$$-V_{i'j'}^0 = \int_{j'}^{i'} \mathbf{E}^0 \cdot d\mathbf{s} \quad (2.89)$$

we can write Eq. (2.84) as

$$Z_{ij}^{int} I_{ij}^n - V_{i'j'}^0 + \frac{I_{ij}^n l i \omega \mu_0}{2\pi} \ln \left( \frac{h + 2p}{h} \right) - (U_i^c - U_j^c) \quad (2.90)$$

where  $l$  is the length of the transmission line segment.

Let us next investigate the right-hand side of Eq. (2.83). By using a harmonic time dependence ( $e^{i\omega t}$ ), it can be written as

$$-i\omega \int_A \mathbf{B} \cdot d\mathbf{a} \quad (2.91)$$

where the total magnetic field  $\mathbf{B}$  is the sum of two sources  $\mathbf{B} = \mathbf{B}^0 + \mathbf{B}^n$ , where  $\mathbf{B}^0$  is the geomagnetic variation field in the absence of the transmission line and  $\mathbf{B}^n$  is the magnetic field produced by the currents flowing along the transmission line. The  $\mathbf{B}^n$ -related term can again be estimated by assuming the field to be produced by an infinite line current and integrating the field

from the surface of the Earth to the surface of the transmission line. This yields

$$-i\omega \int_A \mathbf{B}^n \cdot d\mathbf{a} = -\frac{I_{ij}^n li\omega\mu_0}{2\pi} \ln\left(\frac{h}{r_0}\right) \quad (2.92)$$

where  $h$  is the distance from the center of the transmission line wire to the surface of the Earth and  $r_0$  is the radius of the wire.

The  $\mathbf{B}^0$ -related term in Eq. (2.91) can be estimated assuming a plane wave source, a uniform Earth and negligible air conductivity. It follows from Eqs. (2.47) and (2.52) that at the surface

$$b_x = -\frac{\gamma_1}{i\omega} e_y \quad (2.93)$$

where  $\gamma_1 = \sqrt{i\omega\mu_0\sigma}$  when  $\alpha, \beta \rightarrow 0$ . It follows from the condition  $\alpha, \beta \rightarrow 0$  that there is no  $x$ - nor  $y$ -dependence in the electromagnetic field, and from Eq. (2.72) with zero air conductivity ( $\gamma_0 = 0$ ) it follows that above the surface there is also no  $z$ -dependence. Thus, using Relation (2.93) it can be written

$$-i\omega \int_A \mathbf{B}^0 \cdot d\mathbf{a} = -i\omega \int_A B_x^0 da = \frac{h}{p} \int_{i'}^{j'} E_y^0 ds = -\frac{h}{p} V_{i'j'}^0 \quad (2.94)$$

where here  $p$  is equal to  $1/\sqrt{i\omega\mu_0\sigma}$ . If  $p$  is defined as in Eq. (2.74), it is clear that (2.94) is generally valid for all layered Earth structures.

Collecting all terms of Eq. (2.83) together we obtain

$$I_{ij}^n Z_{ij}^{tot} - V_{i'j'}^0 \left(1 - \frac{h}{p}\right) - (U_i^c - U_j^c) = 0 \quad (2.95)$$

where

$$Z_{ij}^{tot} = Z_{ij}^{int} + \frac{li\omega\mu_0}{2\pi} \ln\left(\frac{h+2p}{h}\right) + \frac{li\omega\mu_0}{2\pi} \ln\left(\frac{h}{r_0}\right) \quad (2.96)$$

The internal impedance  $Z_{ij}^{int}$  can be estimated by using the internal impedance for an infinite wire per unit length (see e.g., Jordan, 1950, p. 376). One obtains

$$Z_{ij}^{int} = \frac{li\omega\mu_m}{2\pi r_0 \gamma_m} \frac{I_0(\gamma_m r_0)}{I_1(\gamma_m r_0)} \quad (2.97)$$

where the subscript  $m$  denotes parameters for the metal of which the wire is composed and  $I_0$  and  $I_1$  are the zeroth and the first order modified Bessel functions, respectively.

Now let us investigate the relative importance of different terms in Eq. (2.95). We denote the second term in the right-hand side of Eq. (2.96) by  $Z_{ij}^{ind}$  and the last term by  $Z_{ij}^n$ . For frequencies below 1 Hz and for a homogeneous Earth conductivity  $10^{-2}$  S/m and  $h = 30$  m, the ratio  $|h/p|$  is order of  $10^{-3}$ . Thus the corresponding term in Eq. (2.95) can clearly be neglected. Different terms of Eq. (2.96) have been evaluated numerically for frequencies from 0 to 1 Hz and are shown in Fig. 2.7. The calculations were made with  $\mu_m = 100\mu_0$ ,  $\sigma_m = 10^7$  S/m,  $\sigma = 10^{-2}$  S/m,  $r_0 = 0.03$  m and  $h = 30$  m, which are realistic values for the present setting. It is seen that, although the difference at 1 Hz is not any more orders of magnitude, the  $Z_{ij}^{int}$  term dominates for frequencies below 1 Hz. It is also seen that the real part of  $Z_{ij}^{int}$  is about an order of magnitude larger than the imaginary part up to 0.1 Hz. Furthermore, the real part remains close to its dc value at frequencies below 1 Hz.

The above computations indicate that the inductive coupling between the transmission line and the Earth can in practice be neglected, i.e. our initial assumption is valid. Furthermore, it was also shown that for the majority of geomagnetic variations, a dc treatment of the GIC flow in a transmission line is justified, although some errors may result from neglecting the imaginary part of  $Z_{ij}^{int}$  when approaching frequencies of the order of 1 Hz. Consequently, we proceed by approximating Eq. (2.95) as

$$I_{ij}^n R_{ij} - V_{ij}^0 - (U_i^c - U_j^c) = 0 \quad (2.98)$$

where  $R_{ij}$  is the dc-resistance of the transmission line between points  $i$  and  $j$  and for convenience we have now marked  $V_{i'j'}^0 = V_{ij}^0$ . Using Kirchhoff's law we can write

$$I_i^e = \sum_{j \neq i} I_{ji}^n = - \sum_{j \neq i} I_{ij}^n \quad (2.99)$$

By substituting  $I_{ij}^n$  in Eq. (2.98) into Eq. (2.99) we obtain

$$I_i^e = - \sum_{j \neq i} \frac{V_{ij}^0}{R_{ij}} - \sum_j Y_{ij} U_j^c \quad (2.100)$$

where the network admittance matrix is defined as

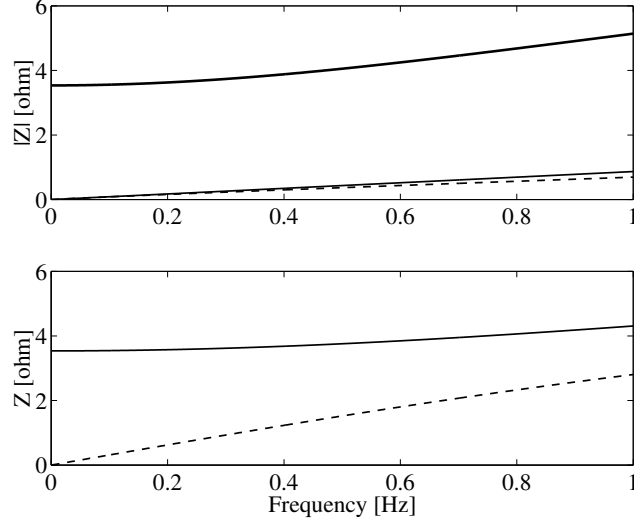


Figure 2.7: Relative importance of different terms in Eq. (2.96). In the top panel  $|Z_{ij}^{int}|$  (heavy solid line)  $|Z_{ij}^n|$  (dashed line) and  $|Z_{ij}^{ind}|$  (thin solid line) for frequencies from 0 to 1 Hz are presented. In the bottom panel the real (solid line) and imaginary (dashed) parts of  $Z_{ij}^{int}$  are shown. See text for details.

$$Y_{ij} = \begin{cases} -\frac{1}{R_{ij}} & i \neq j \\ \sum_{k \neq i} \frac{1}{R_{ik}} & i = j \end{cases} \quad (2.101)$$

And finally, using Relation (2.86) we obtain the solution for the earthing current vector

$$\mathbf{I}^e = (\mathbf{1} + \mathbf{Y}\mathbf{Z}^e)^{-1} \mathbf{J}^e \quad (2.102)$$

where

$$J_i^e = - \sum_{j \neq i} \frac{V_{ij}^0}{R_{ij}} \quad (2.103)$$

Relations (2.86), (2.98) and (2.102) permit the calculation of the currents anywhere in the transmission system if the electrical parameters  $Z_{ij}^e$ ,  $R_{ij}$  and the topology of the system and the geoelectric field  $\mathbf{E}_0$  are known.



### 2.3.2 Continuously grounded systems

The treatment of a continuously grounded systems is quite different from the treatment of discretely grounded systems. The details can be found in Paper I and thus only a brief overview is given here. Again, although we discuss here buried pipelines, the same treatment is valid for all continuously grounded systems.

We aim to model pipeline *networks*. Simplified pipeline models, like an infinitely long cylinder (see e.g., Ogunade, 1986; Trichtchenko and Boteler, 2001) are treated otherwise. The basic idea in modeling a pipeline network is to represent a segment of the pipeline as a transmission line having a source embedded in it (see Fig. 2 in Paper I). This makes it possible to model the pipeline as a distributed source transmission line (DSTL) and to use methods familiar from the transmission line theory (e.g., Smith, 1987).

From the DSTL theory we obtain the following equation describing the current flow  $I(x)$  within a uniform pipeline section

$$\frac{d^2 I(x)}{dx^2} - \gamma_p^2 I(x) = -Y_p E_0(x) \quad (2.104)$$

where  $\gamma_p = \sqrt{Z_p Y_p}$  and  $Z_p$  and  $Y_p$  are the parallel impedance and the transverse admittance per unit length of the pipeline and are not to be confused with the spectral impedance treated in Section 2.2 or with the earthing impedance matrix and the network admittance treated in Section 2.3.1.  $\gamma_p$  is effectively the adjustment distance over which discontinuities in the pipeline affect the current flow  $I(x)$ . Similar to discretely grounded systems,  $Z_p$  is in practice the dc-resistance of the pipeline metal per unit length and  $Y_p$  is the dc-admittance of the pipeline coating (from the pipeline metal to the ground), thus permitting a dc treatment also for pipelines. The validity of the dc assumption is tested and discussed Paper I. Conclusions are again similar to those made for discretely grounded systems: For frequencies of the order of 0.01 Hz or less the dc assumption is perfectly valid, but when approaching frequencies of the order of 1 Hz some errors may be introduced if  $Z_p$  and  $Y_p$  are kept as dc quantities. However, errors due to the dc treatment are clearly not large enough to justify the burden of a full ac treatment of the problem.

Eq. (2.104) has a simple solution for a single pipeline section. The principal idea in modeling the discontinuities of the pipeline network is to solve (2.104) for each section separately and to embed the rest of the network inside an equivalent terminating impedance and a voltage source, i.e. boundary conditions of the section in question. The equivalent impedance

and the voltage source are computed using the *Thevenin theorem* (e.g., Ferris, 1962). By constructing the boundary conditions one by one recursively starting from the ends of the network until the end of the section under consideration, we are able to determine the current and the pipe-to-soil voltage profiles along the entire pipeline network.

## 2.4 Unification of the methods for practical applications

Here a general method applicable for computation of GIC in technological conductor systems on the ground is introduced. It is assumed that magnetic field data from a sufficiently large number of stations is available and that the overall ground conductivity structure, the topology of the system and the electrical dc parameters of the system are known.

Fig. 2.8 presents the flow of different steps of the method. The input to each model together with the model output are shown. First, the SECS method (Section 2.1) is applied to geomagnetic field data from a set of measurements to derive the ionospheric equivalent currents. The ionospheric equivalent currents are then used to compute the magnetic field at any desired point at the surface of the Earth. In the next step, the geoelectric field is computed using the surface impedance, calculated using the information from the ground conductivity, as described in Section 2.2.1. Finally, the geoelectric field and the network data is used to compute GIC in any part of the conductor system by applying the methods presented in Sections 2.3.1 and 2.3.2. Note that the method can be used also for real-time computations thus permitting nowcasting of GIC.

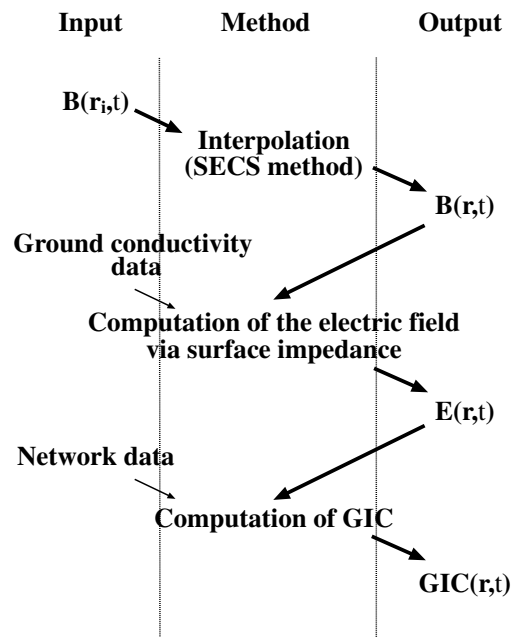


Figure 2.8: Flow of different steps used in the practical calculation of GIC in technological conductor systems on the ground. See text for details.



## Chapter 3

# Characteristics of intense GIC events

### 3.1 Properties of intense meso-scale geoelectric fields

As was seen above, if the electrical parameters and topology of the technological conductor system under investigation and the surface geoelectric field are given, we are able to determine GIC in all parts of the system. Thus it is clear that we need to understand the basic nature of the geoelectric field in order to understand the behavior of GIC. As only large GIC are of interest to us, the main attention is paid to intense geoelectric fields ( $> 100$  mV/km). The reason why we are interested in meso-scale ( $\sim 100$  km) fields is that due to integration of the geoelectric field made in calculating (and creating) GIC, formally seen from Eq. (2.89) in Section 2.3 and Eqs. (18) and (19) of Paper I, small-scale ( $\sim 1$  km) features in the geoelectric field smooth out and are thus not very important from the GIC viewpoint. This is an important and simplifying feature in GIC studies since the small-scale electric field is very much dependent on the local conductivity structure which, especially in the uppermost layers, can be highly varying. If such regions are taken into account, the assumption about locally laterally homogeneous conductivity structures used in Section 2.2 would be violated and the modeling of the geoelectric field would become much more complicated. However, it should be noted that, for example, in the cases of ocean-continent boundaries and small scale anomalies with very high conductivity contrast to the background conductivity, assumption about the lateral homogeneity is so severely distorted that more sophisticated methods are required for the es-

timation of the GIC-associated geoelectric field.

Perhaps the greatest general misconception connected with GIC is the presumption about the east-west preference of the auroral geoelectric fields. If longitudinally uniform auroral ionospheric currents are assumed to flow only in the east-west direction and the ground conductivity is laterally uniform, the assumption is acceptable. However, as shown by Viljanen (1997) and Viljanen et al. (2001), the time derivatives of the ground magnetic field, and thus via Relations (2.66)-(2.67) also the ground geoelectric field, can have large values in any direction. This means that the source for large time derivatives is more complicated than just a simple east-west oriented electrojet. An example of this fact is seen in Fig. 3.1 where the modeled and the measured GIC in the Finnish pipeline at Mäntsälä and the time derivative of the north and east components of the ground magnetic field at the Nurmijärvi Geophysical Observatory on September 8, 2002 are shown. It is seen that this time GIC closely follows the behavior of the time derivative of the east component of the magnetic field ( $dB_y/dt \sim E_x$ , see Section 2.2.1), whose magnitude is about twice as large as the magnitude of  $dB_x/dt (\sim E_y)$ . The modeled GIC is computed with the method described in Section 2.3.2 and in Paper I.

Having large values of ground geoelectric field to any direction, it is natural to think that there may be further complications related to the "electrojet-thinking", namely issues associated with the spatial scales of the surface geoelectric fields. This has been investigated in Papers III and IV. Again only a brief summary is given here, for details see the attached papers. Looking at the times of large GIC or large time derivatives of the magnetic field, it was shown that the cases studied were imposing various types of behavior of the geoelectric field, spatial scales of the fields varying from thousands of kilometers to less than one hundred kilometers. Patterns of the geoelectric fields were also varying to high degree, being dependent on the type of the ionospheric source. Thus, although spatial scales of about 100 km and above are of main interest, already 100 km is a relevant scale for understanding the true sources of large GIC. The temporal scales related to intense geoelectric fields were seen to be relatively short, varying from about 10 minutes down to 1 minute and even less. Thus the periods of our interest are roughly within the range of 1-600 seconds, longer period fields are not effective enough, i.e. do not have large enough amplitudes, to produce notable GIC. This feature is also seen from the example shown in Fig. 3.1 where the longest period of the largest GIC is about 600 seconds.

The temporal scales discussed above have important implications for the requirements of the ground conductivity models to be used when computing

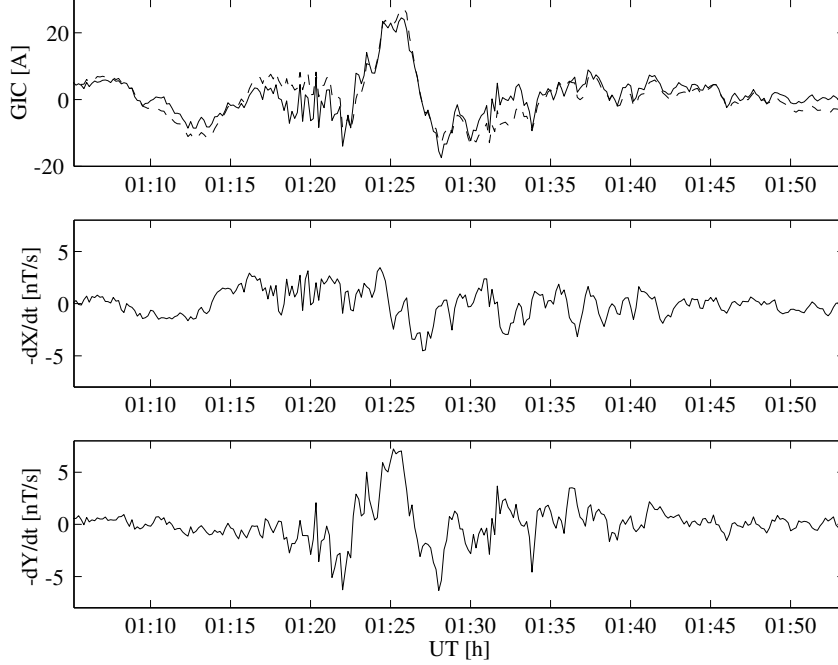


Figure 3.1: Modeled (dashed) and measured GIC in the Finnish pipeline at Mäntsälä and the time derivative of the north ( $X$ ) and east ( $Y$ ) components of the ground magnetic field at Nurmijärvi Geophysical Observatory on September 8, 2002.

GIC. The skin depth  $\delta$  is defined using the solution for the electromagnetic field in a homogeneous Earth presented in Eq. (2.43). The behavior of the field in the Earth is connected to the parameter  $\gamma$  (wave number) which can be presented as

$$\gamma = \sqrt{i\omega\mu_0\sigma} = \frac{1}{\delta} + i\frac{1}{\delta} \quad (3.1)$$

where  $\delta = \sqrt{2/\omega\mu_0\sigma}$  is the skin depth characterizing the evanescence of the field in the medium. From the exponential term of Eq. (2.58) it is seen that  $\delta$  also characterizes the decay of the kernel function in Eq. (2.54) used to derive the surface geoelectric field from ground magnetic field variations. By varying the periods between 1 to 600 seconds and the conductivities from 1 to  $10^{-3}$  S/m,  $\delta$  takes on values between 0.5 and 400 km. This again indicates the relatively local character of the GIC-associated electromagnetic field. Thus it is quite clear that in order to investigate GIC in a certain

region, meso-scale ( $\sim 100$  km) Earth conductivity models are applicable. This justifies, for example, the approach used in the work by Pulkkinen et al. (2000) where local conductivity models were used to compute the regional geoelectric fields via Eqs. (2.66)-(2.67).

On the other hand, small spatial scales of the geoelectric fields at auroral latitudes indicate that the ground electromagnetic fields or the ionospheric source cannot be reliably interpolated or extrapolated to great distances, unlike in the case of a one-dimensional electrojet. In order to compute trustworthy GIC estimates, one needs information about the source from the immediate vicinity of the region of interest. Note that this requirement can possibly be relaxed at lower latitudes where the source is likely to be more uniform. For example in the study by Koen (2002), GIC in the Southern African (mid-latitudes) power transmission system was modeled relatively accurately by using ground magnetic data from the Hermanus Geomagnetic Observatory located 500 kilometers from the GIC measurement site.

How the discussed properties of the ground geoelectric fields relate to actual GIC has been studied using the methods presented in Chapter 2 for example by Viljanen et al. (1999), Pulkkinen et al. (2000) and in Paper II. In the work of Pulkkinen et al. (2000), GIC in the Finnish power transmission system were studied. In the work, a uniform regional block conductivity models of Finland and geomagnetic data from the IMAGE magnetometer array from the years 1993-1999 were used to calculate the geoelectric field via Eqs. (2.66)-(2.67). The geoelectric field was then used as input to the model of the transmission system (see Section 2.3.1) giving GIC at different parts of the system. Fig. (3.2) depicts the distribution of the lengths of the peaks during which the sum of the absolute values of GIC through the transformers of the Finnish high-voltage power system exceeds 400 A. The distribution is based on 173 events during which the geomagnetic  $K$  index<sup>1</sup> at Nurmijärvi Geophysical Observatory reached the value 9. All events last less than 10 minutes, supporting the conclusions about the relevant periods made above. It is also seen that the number of large events is peaked at durations of less than one minute.

In Fig. 3.3 the geoelectric field pattern and the corresponding GIC in the Finnish power transmission system are shown for an event on April 7, 1995, the time of the snapshot is 16:47 UT. The figure shows a good example of the fact that although the spatially small scale features are of a great importance, large GIC can be observed throughout the network at the same time. In this sense, large events exhibit both small and large-scale features,

---

<sup>1</sup>three-hour geomagnetic activity index (scale 0-9)



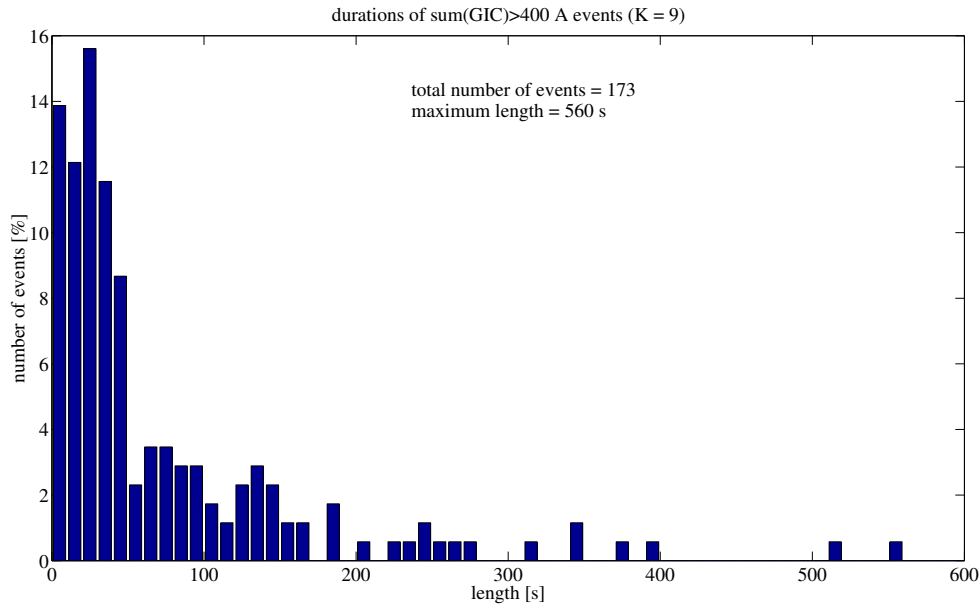


Figure 3.2: Distribution of the lengths of peaks during which the sum of GIC through the transformers of the Finnish high-voltage power system exceeds 400 A. Events with  $K=9$  during years 1993-1999 are considered. Figure adopted from Pulkkinen et al. (2000).

and thus it is difficult to point out any specific section that is most affected by GIC during each time instant.

In Paper II, the conductivity model of southern Finland and geomagnetic data from Nurmijärvi Geophysical Observatory for years 1993-2001 were used to calculate the geoelectric field at the surface of the Earth again via Eqs. (2.66)-(2.67). The computed geoelectric was then used as input to the model of the Finnish pipeline network (see Section 2.3.2) giving GIC at different parts of the network. Statistics were derived to find the parts of the pipeline most affected by GIC. For details, see the attached paper. In connection with this work measurements of GIC in the Finnish pipeline at Mäntsälä were started in November 1998. Measurements have continued since then, making up a unique dataset for GIC studies. The latest statistics of these measurements are shown in Fig. 3.4 where the occurrence of GIC (November 13, 1998 - February 19, 2003) is shown. The largest measured GIC so far is about 32 A. Fig. 7 of Paper II where the modeled occurrence is shown, suggests that 32 A can be more than doubled at Mäntsälä during

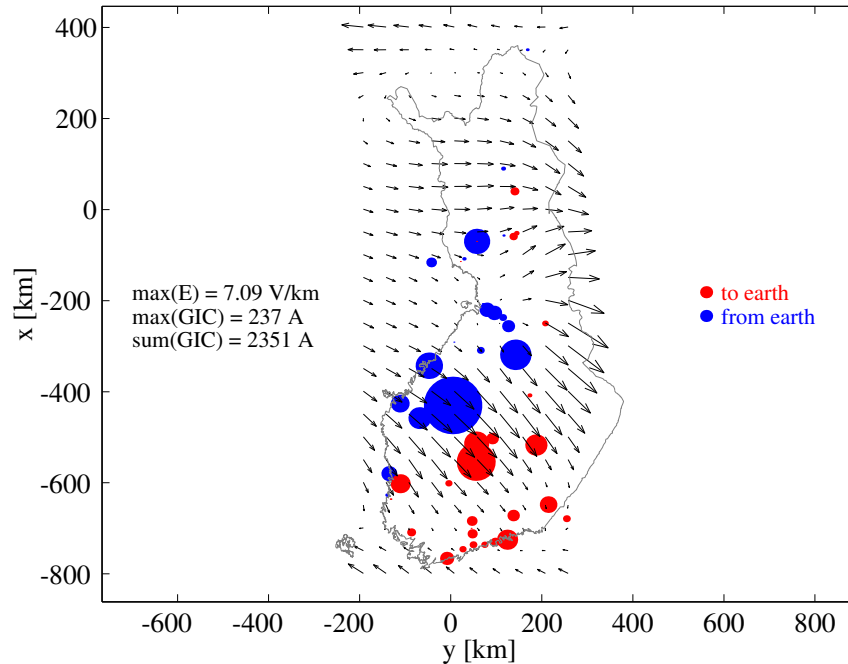


Figure 3.3: Snapshot of geoelectric field (arrows) computed from the ground magnetic data and the corresponding computed GIC (circle) distribution during an intense event on April 7, 1995 at 16:47 UT. The radius of the circle correspond to the magnitude of GIC flowing through the neutrals of the power transformers. Figure adopted from Pulkkinen et al. (2000).

the very largest GIC events.

### 3.2 Properties of ionospheric currents causing intense geoelectric fields and the linkage to large-scale magnetospheric phenomena

The primary driver of the geoelectric field in the auroral regions is the ionospheric electric current system which in turn is connected to the large-scale magnetospheric and solar wind dynamics (see Fig. 1.2). Thus, the next natural step is to look at the ionospheric dynamics related to large GIC, and then ultimately extend this to cover the magnetospheric phenomena in general. These goals demonstrate again quite well the interdisciplinary

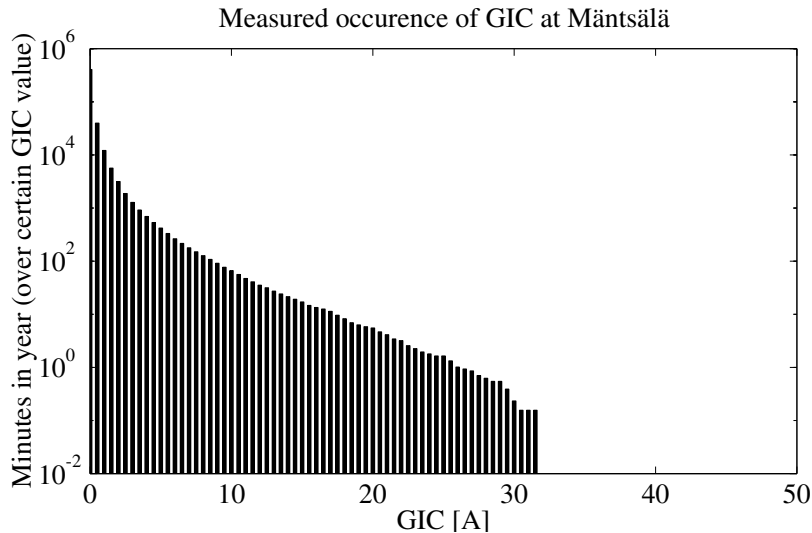


Figure 3.4: Distribution of occurrence frequency of measured GIC in the Finnish pipeline system which exceed a given GIC threshold (observation interval Nov 13, 1998 - Feb 19, 2003).

nature of GIC studies.

It has been known for a while that GIC are driven by rapid variations of ionospheric currents (e.g., Akasofu and Merrit, 1979). At high latitudes, where the most intense GIC are experienced, these variations are thought to be related to the intensification of the electrojets during enhanced ionospheric convection conditions and to the development of the substorm current wedge during geomagnetic substorms. However, despite numerous studies of GIC, there still exists no well-established picture of the detailed structure of the ionospheric currents driving the largest GIC. Some rough estimates of the electrojet intensity and morphology during GIC events have been carried out (e.g., Mäkinen, 1993; Bolduc et al., 1998, 2000; Boteler, 2001b) and the connection of large GIC to magnetospheric and solar phenomena has been documented (Lam et al., 2002), but no rigorous study of realistic ionospheric source currents is available to date. A lot of recent GIC investigations are still relying on the old fashioned (though valid as a first approximation) assumption about a one-dimensional electrojet source put forward in GIC studies by authors like McNish (1940); Albertson and Van Baelen (1970).

We investigate the GIC-related dynamics using ionospheric equivalent

currents which are derived using the spherical elementary current system method as explained in Section 2.1. The approach contains the computation of equivalent currents for periods during which intense induction effects are experienced, and an investigation of the derived current patterns. The primary aim is to shed light on the detailed structure of the source, and ultimately to understand the relation to the magnetospheric and solar wind conditions. The work has been started in the investigations presented in Papers III and IV. In Paper III, the usage of two-dimensional ionospheric equivalent currents in GIC studies was introduced and ionospheric sources for large geoelectric fields during the disturbed period on June 26, 1998 were investigated. In Paper IV, the same approach was extended to cover the entire Sun - solar wind - magnetosphere - ionosphere - ground chain for the April 6-7, 2000, geomagnetic storm event by using the study by Huttunen et al. (2002) as a background. Findings of these investigations are briefly summarized and discussed below.

The June 26, 1998, period (01:18 - 01:48 UT) coincided with a substorm expansion phase (on substorms see e.g., Rostoker, 1996; Tanskanen, 2002) during which three different clearly identifiable ionospheric features were seen to cause intense geoelectric fields. These were an Omega band event (on Omega bands see e.g., Amm, 1996), a relatively smooth intensification of the westward electrojet and a combined enhancement and turning of ionospheric equivalent currents. Thus even during a relatively short, 30-minute, period several ionospheric causes for large GIC were seen, all coinciding with a single auroral substorm. The same was observed in the April 2000 storm when the largest GIC were clearly associated with substorms. However, during both the June 1998 and April 2000 events, there were no common characteristics in the substorm behavior that can be associated with these events: The actual causes were typically complex structures embedded in the substorm-associated temporal development of the larger scale current systems. Anyhow, the presence of the auroral electrojet in general favored large GIC. A sketched illustration of these features is shown in Fig. 3.5. It is noted that isolated substorms occur without actual geomagnetic storm. Accordingly, large GIC can also occur without notable "background" geomagnetic activity.

Though substorms are possibly the most typical causes for the largest GIC in the auroral region, they by no means are the only cause. During the April 2000 geomagnetic storm also sudden commencement and geomagnetic pulsations were seen to cause large GIC. Furthermore, large GIC can occur at any time of the day. An example of this is seen in Fig. 3.6 where GIC in the Finnish pipeline and magnetic field data from the northern hemisphere

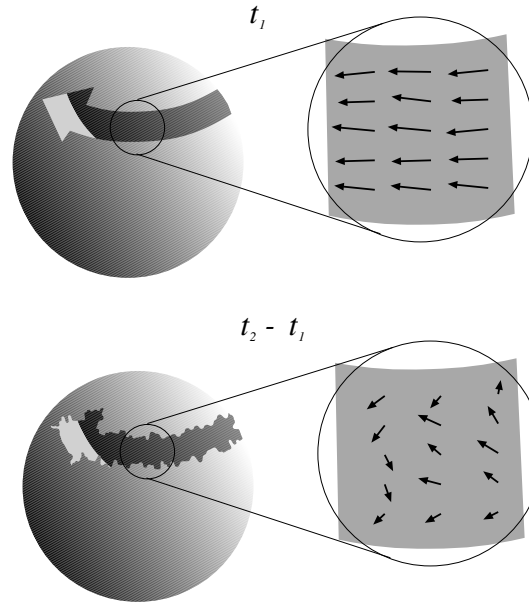


Figure 3.5: Graphical illustration of typical auroral ionospheric current characteristics behind large GIC. On the top: intensified electrojet at time  $t = t_1$ . Generally  $|J_y| \gg |J_x|$ , i.e. on the ground  $|B_x| \gg |B_y|$ . On the bottom: differential currents ( $t_2 - t_1$ ) producing the surface geoelectric field. Generally  $|dJ_y/dt| \approx |dJ_x/dt|$ , i.e. on the ground  $|dB_x/dt| \approx |dB_y/dt|$ .

are shown for the geomagnetic storm that occurred on November 24, 2001. The GIC peak was observed at 07:14 UT (Finnish local time is UT + 2 hours), i.e. during the daytime. Though the cusp probably itself is not over Finland at this time, the peak value is caused by the very dynamic changes in the cusp related ionospheric current system (see e.g., Kamide and Baumjohann, 1993, p. 26-30) in the vicinity of Mäntsälä. As is seen from the figure, intense disturbances were observed at the same time throughout the northern hemisphere. The November 2001 event will be investigated in a forthcoming paper.

In terms of auroral substorms, the connection of large GIC to large-scale magnetospheric dynamics naturally falls into basic mechanisms of substorms. The problem is that from the GIC viewpoint we are interested in effects of relatively small temporal and spatial scales, and at the moment even the most fundamental mechanisms of the substorm processes are not well known. Possible self organized criticality and the associated non-linearities

in substorm phenomena (e.g., Klimas et al., 2000) may ultimately imply that the detailed dynamics are far too complex to be modeled in greater detail. If that is the case, it also sets restrictions for the ultimate accuracy of GIC modeling initiated from first principle magnetospheric models. However, events like sudden commencements and certain types of geomagnetic pulsations are, though non-linear processes, thought to be directly solar wind driven and are less structured in terms of the ground magnetic signature (e.g., Araki, 1994; Chisham and Orr, 1997), implying that the evolution of these events may be easier to be modeled thus enabling accuracy sufficient for GIC-related purposes. Anyhow, it is clear that more needs to be known about the relative importance of different ionospheric processes behind large GIC and about the linkage of the dynamics to magnetospheric phenomena before any more definite conclusions about these issues can be drawn. The extension of the work made here is one of the main keys to a deeper understanding of GIC phenomena.

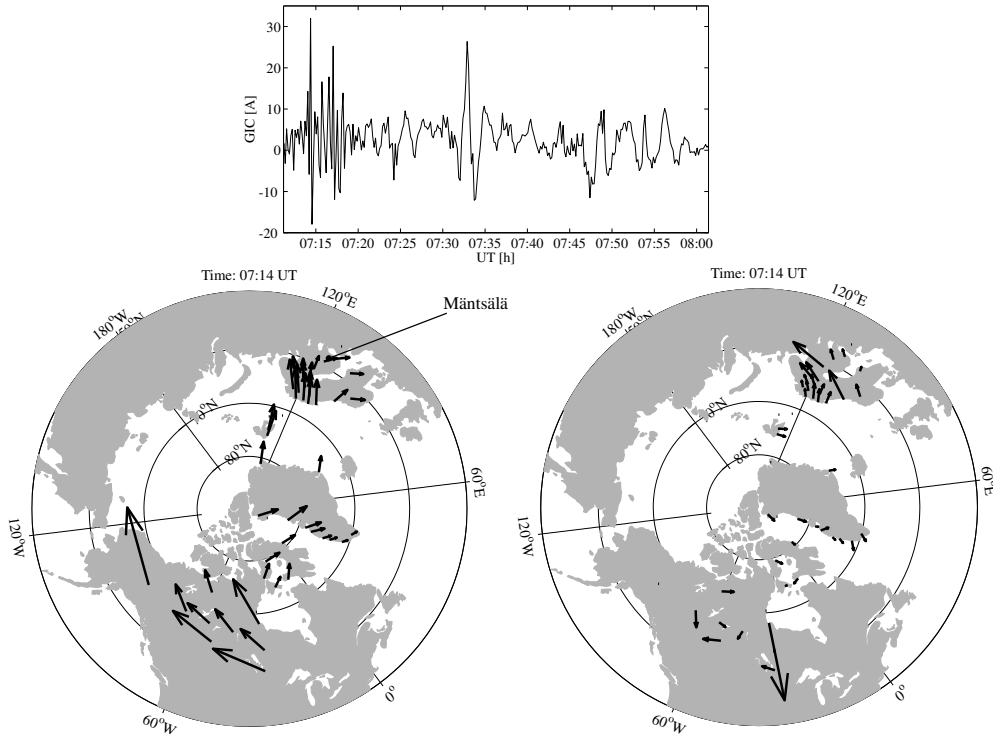


Figure 3.6: Geomagnetic storm event on November 24, 2001. On the top: GIC measured in the Finnish pipeline at Mäntsälä. The peak GIC is measured at 07:14 UT. On the bottom, on the left: 90 degrees clockwise rotated horizontal magnetic field vectors ( $\sim \mathbf{J}_{eq}$ ) at 07:14 UT. Max  $|\mathbf{B}_{hor}| = 2641$  nT. On the bottom, on the right: 90 degrees anticlockwise rotated  $d\mathbf{B}_{hor}/dt$  ( $\sim \mathbf{E}$ ) at 07:14 UT. Max  $|d\mathbf{B}_{hor}/dt| = 15$  nT/s as computed from one minute values. Geomagnetic (dipole) coordinates are used.





# Chapter 4

## Discussion

### 4.1 Theses of the work

We have browsed through the field of GIC. We started from the motivation of the research by looking at how GIC affects our everyday life and continued to relate GIC to a more general context of space weather and ultimately to the context of the solar-terrestrial and solid Earth physics. Then we took a look at the mathematical models relevant for GIC research. Separate set of methods were given for treating the geophysical and engineering parts of the problem. Finally, we investigated the basic characteristics of the geoelectric field driving large GIC and the properties of the ionospheric and magnetospheric phenomena behind the field. There are several theses that emerge from these considerations. The essence of the theses and the novel work behind these theses are the following:

- GIC research is the interface between the solid Earth and space physics domains. There are a number of lessons to be learned through this interface.

Novel work: Geomagnetically induced currents were investigated utilizing methods and knowledge both from the solid Earth and space physics.

- GIC can be modeled relatively accurately with rather simple mathematical tools requiring that the topology and the electrical parameters of the system, the ground conductivity structure and either the ionospheric source current or the ground magnetic field variations are known.

Novel work: A model for computing GIC in any pipeline network was developed and applied to the Finnish pipeline. The dc treatment of GIC was validated for both continuously and discretely grounded systems. The SECS method was introduced to GIC studies and the method was used for developing a new magnetic field separation technique. The combined usage of the SECS method and CIM was introduced. The surface impedance technique for computing the geoelectric field from the ground magnetic field was analytically transformed from the spectral to the spatio-temporal domain. A new practical method for computing GIC in any technological conductor system was introduced.

- From the geophysical viewpoint, the character of GIC events is twofold. On one hand, large GIC can be observed at the same time instant throughout the entire auroral region. On the other hand, spatial and temporal scales related to these events are rather small making the detailed behavior of individual GIC relatively local.

Novel work: Two geomagnetically disturbed periods were investigated in detail both from the geoelectric field and the ionospheric equivalent current viewpoint. A large set of magnetic data was utilized for comprehensive two-dimensional view of the characteristics of the phenomena.

- Though substorms are statistically the most important drivers of large GIC in the auroral region, there are a number of different magnetospheric mechanisms capable to produce dynamic changes which result in large GIC.

Novel work: A geomagnetic storm was investigated throughout the Sun - solar wind - magnetosphere - ionosphere - ground - GIC chain, and dynamics in the magnetosphere-ionosphere system causing the largest GIC of the event were identified.

## 4.2 New challenges

The work presented here gives rise to many questions and challenges that need to be considered in coming GIC studies. Some of these are highlighted.

It was shown that under typical geomagnetic conditions the existing mathematical methods are sufficient for a fairly accurate GIC modeling. However, there are occasions in which some of the assumptions, namely the

one-dimensional Earth conductivity structure, linear variations of the source field within the effective area of the operator  $G(x', y', t')^0$  (Section 2.2.1) or smoothness of the source field compared to the complex skin depth related to the image source ( $|(\eta p)|^3 \ll 1$  condition in Section 2.2.2) are violated. Such occasions may occur for example at the ocean-continent boundaries and during events when a highly structured ionospheric source current varies relatively slowly in time. In such cases a full three-dimensional treatment of the induction problem with true sources is required. The extension of the work by Engels et al. (2002) combined with the field separation presented in Section 2.1.1 provide efficient tools for the treatment. The approach is as follows: 1.) The data from the Baltic Electromagnetic Array Research (BEAR) period (June - July 1998) during which the magnetic field was recorded in a dense array covering the Fennoscandia (Korja et al., 2002) are used. The same data were utilized in Papers III and V. The BEAR data are separated to get the best estimate for the ionospheric equivalent source, 2.) A three-dimensional induction code is run for relevant periods using the Fennoscandian conductivity model and the derived ionospheric source, 3.) The output from the modeling is analyzed. In addition to GIC related issues, this work will provide important information about source distortions in the magnetotelluric modeling and about distortions caused by the ocean-continent boundaries in magnetic field recordings.

As was discussed in Introduction, GIC forecasting can be considered as an ultimate test for our understanding of the solar-terrestrial environment. Thus, the current status of different forecasting methods is of great interest from both the scientific and the commercial viewpoint (for a description of already existing GIC forecast service see Kappenman et al. (2000)). For example, some mitigation procedures could be applied if advance warnings were provided for power transmission system operators (Molinski, 2002). The forecasting methods that come into question are the "first principle" magnetohydrodynamic (MHD) modeling of the magnetosphere-ionosphere system and the "black box" neural network and other non-linear filter techniques for creating empirical transfer functions between solar wind plasma parameters and ground magnetic field variations (for a review see e.g., Lundstedt, 1997; Detman and Vassiliadis, 1997). Such methods have been implemented for example in the MHD code by Janhunen (2000) and in a neural network model by Weigel et al. (2003). Though the MHD code cannot yet be run faster than real-time, i.e. cannot be applied to real forecasts, it is interesting to check if the code is able to reproduce features in the ground magnetic field of any use for GIC purposes. This and the performance of the model by Weigel et al. (2003) will be evaluated in the near-future study us-

ing the data and experience from the April 2000 event that was discussed in Section 3.2. It should be noted that it is not realistic to anticipate one-to-one correspondence between observed and modeled GIC but rather indications of regions where GIC activity may be expected.

To draw more quantitative conclusions about the relative importance of different ionospheric drivers of large GIC discussed in Section 3.2, a rigorous classification of a large number of GIC-related current systems is required. For large datasets, and because of the need for objectivity and the time used in the analysis, this calls for automatized procedures in practice. Interestingly, there is some experience on the identification of auroral forms using pattern recognition techniques (Syrjäsuo, 2001). In principle, the problem of identifying ionospheric current structures, for example in terms of derived scaling factors of elementary systems (discussed in Section 2.1), is rather close to the identification of auroral images. Thus, it would be very interesting to try to transform the ideas of pattern recognition also to the ionospheric current detection and classification. This type of work would naturally benefit solar-terrestrial physics in general.

It is quite clear that only the very largest GIC, like those experienced during the March 1989 event, are capable of producing such large effects that catastrophic failures of systems on the ground are possible. So, it is of great interest not only to estimate by using the existing data how often these types of extreme events have occurred but also to try to extrapolate these data to conclude how intense events are possible to occur. As indicated by Langlois et al. (1996), there probably exists some constraints in the dynamics of the magnetosphere-ionosphere system that also give limit to the largest possible geoelectric fields and GIC. One constraint is set by the characteristics of the storm driver, i.e. the most extreme solar ejecta (see e.g., Tsurutani, 2001). Other natural constraints could be related, for example, to the largest possible energies released in substorms and to the shortest possible time scales associated with the release. Fig. 4.1 shows the statistical occurrence of the total horizontal geoelectric field  $|\mathbf{E}|$  at the Nurmijärvi Geophysical Observatory during years 1993-2001. The geoelectric field was computed using Relations (2.66)-(2.67) with a ground conductivity  $\sigma = 3.1 \cdot 10^{-2}$  S/m estimated in Paper II. It can be seen that the occurrence of large geoelectric fields follows a power-law pattern, characteristic for systems exhibiting self organized criticality (e.g., Klimas et al., 2000). If data for a long enough period would exist, the constraint mechanism would cause a possibly abrupt drop in the curve. Such a drop is not evident in the statistics of Fig. 4.1, and it would be interesting to speculate how far down up the higher geoelectric field values the power law holds.

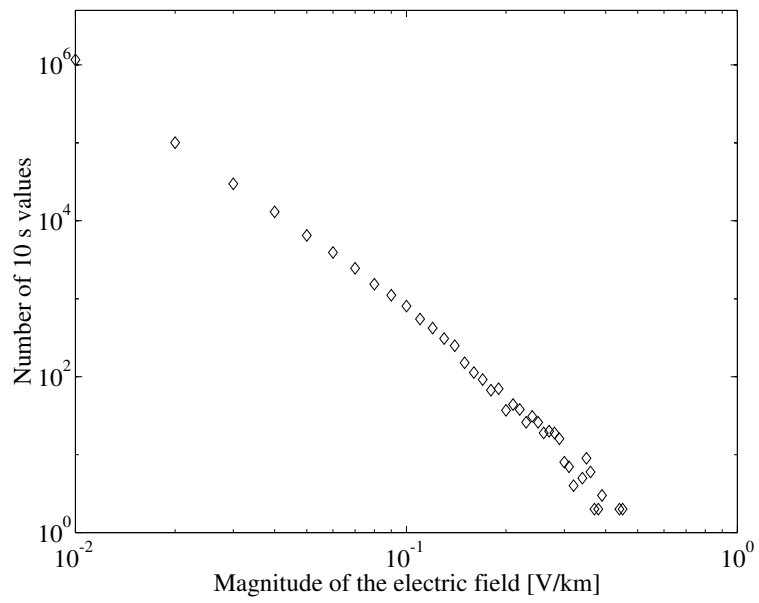


Figure 4.1: Occurrence of the computed total horizontal geoelectric field  $|\mathbf{E}|$  at Nurmijärvi Geophysical Observatory during years 1993-2001.



# Bibliography

- Akasofu, S.-I., and R.P. Merrit, Electric currents in power transmission line induced by auroral activity, *Nature*, **279**, 308, 1979.
- Albertson, V., and J. Van Baelen, Electric and magnetic fields at the Earth's surface due to auroral currents, *IEEE T. Power Ap. Syst.*, **89**, 578, 1970.
- Amm, O., Improved electrodynamic modeling of an omega band and analysis of its current system, *J. Geophys. Res.*, **101**, 2677, 1996.
- Amm, O., Ionospheric elementary current systems in spherical coordinates and their application, *J. Geomagn. Geoelectr.*, **49**, 947, 1997.
- Amm, O., and A. Viljanen, Ionospheric disturbance magnetic field continuation from the ground to ionosphere using spherical elementary current systems, *Earth, Planets and Space*, **51**, 431, 1999.
- Amm, O., The elementary current method for calculating ionospheric current systems from multisatellite and ground magnetometer data, *J. Geophys. Res.*, **106**, 24843, 2001.
- Anderson, C.W., L.J. Lanzerotti, and C.G. MacLennan, Outage of the L-4 System and the Geomagnetic Disturbances on August 4, 1972, *Bell Syst. Tech. J.*, **53**, 1817, 1974.
- Anderson, C.W., Magnetic storms and cable communications, *Solar System Plasma Physics*, ed. Kennel, C.F., Lanzerotti, L.J., and Parker, E.N., North-Holland, Amsterdam, 1978.
- Araki, T., A physical model of the geomagnetic sudden commencement, *Solar Wind Sources of Magnetospheric Ultra-Low-Frequency Waves, Geophys. Monogr. Ser.*, **81**, edited by M.J. Engebretson, K. Takahashi, and M. Scholer, 183 p., AGU, Washington, D.C., 1994.

- Arfken, G., and H. Weber, Mathematical methods for physicists, *Academic Press*, 4th Ed., 1995.
- Barlow, W.H., On the Spontaneous Electrical Currents Observed in Wires of the Electrical Telegraph, *Phil. Trans. Roy. Soc., London*, **139**, 61, 1849.
- Barnes, P.R., and J.W. Van Dyke, Economic Consequences of Geomagnetic Storms (a summary), *IEEE Power Engineering Review*, November, 1990.
- Berdichevsky, M., and M. Zhdanov, Advanced theory of deep geomagnetic sounding, *Elsevier Science Publishers B.V., Netherlands*, 408 pp., 1984.
- Bolduc, L., P. Langlois, D. Boteler, and R. Pirjola, A Study of Geoelectromagnetic Disturbances in Québec, 1. General Results, *IEEE Trans. Power Delivery*, **13**, 1251, 1998.
- Bolduc, L., P. Langlois, D. Boteler, and R. Pirjola, A Study of Geoelectromagnetic Disturbances in Québec, 2. Detailed Analysis of a Large Event, *IEEE Trans. Power Delivery*, **15**, 272, 2000.
- Bolduc, L., GIC observations and studies in the Hydro-Québec power system, *J. Atmos. Sol.-Terr. Phys.*, **64**, 1793, 2002.
- Boteler, D., and M.J. Cookson, Telluric currents and their effects on pipelines in the Cook Strait region of New Zealand, *Materials Performance*, 27, March, 1986.
- Boteler, D.H., and R.J. Pirjola, The complex-image method for calculating the magnetic and electric fields produced at the surface of the Earth by the auroral electrojet, *Geophys. J. Int.*, **132**, 1, 31, 1998.
- Boteler, D.H., R.J. Pirjola, and H. Nevanlinna, The Effects of Geomagnetic Disturbances on Electrical Systems at the Earth's Surface, *Adv. Space Res.*, **22**, 17, 1998.
- Boteler, D., Geomagnetic effects on the Pipe-to-Soil Potentials of a Continental Pipeline, *Adv. Space Res.*, **26**, 15, 2000.
- Boteler, D., Geomagnetic hazards, *Synthesis of Geological Hazards in Canada*, ed. G.R. Brooks, *Geological Survey of Canada, Bulletin 548*, 183, 2001a.
- Boteler, D., Space Weather Effects on Power Systems, *Space Weather*, AGU Geophysical Monograph 125, 347, 2001b.



- Brasse, H., and A. Junge, The Influence of Geomagnetic Variations on Pipelines and an Application for Large-Scale Magnetotelluric Depth Sounding, *J. Geophys.*, **55**, 31, 1984.
- Cagniard, L., Basic theory of the magneto-telluric method of geophysical prospecting, *Geophysics*, **18**, 605, 1953.
- Campbell, W.H., Induction of Auroral Zone Electric Currents Within the Alaska Pipeline, *Pure Appl. Geophys.*, **116**, 1143, 1978.
- Carlowicz, M.J., and R.E. Lopez, Storms from the Sun, the emerging science of space weather, *The Joseph Henry Press, Washington, D.C.*, 2002.
- Carrington, R.C., Description of a singular appearance seen in the Sun on September 1, 1859, *Monthly Notices of the Royal Astronomical Society*, **20**, p. 13, 1860.
- Chapman, S., and J. Bartels, Geomagnetism, **Vol. 2**, Clarendon Press, Oxford, 1049 pp., 1940.
- Chisham, G., and D. Orr, A statistical study of the local time asymmetry of Pc 5 ULF wave characteristics observed at midlatitudes by SAMNET, *J. Geophys. Res.*, **102**, 24339, 1997.
- Czech, P., S. Chano, H. Huynh, and A. Dutil, The Hydro-Quebec System Blackout of 13 March 1989: System Response to Geomagnetic Disturbance, *EPRI Report, TR-100450, Proceedings of Geomagnetically Induced Currents Conference*, Millbrae, California, USA, November 8-10, 1989, 1992.
- Daly, E.J., and A. Hilgers, Space Weather: European Space Agency Perspectives, *Space Weather*, AGU Geophysical Monograph 125, 53, 2001.
- Davidson, W.H., The magnetic storm of March 24, 1940 - effects in the power system, *Edison Electric Institute Bulletin*, July 1940, 365, 1940.
- Detman, T., and D. Vassiliadis, Review of techniques for magnetic storm forecasting, *Magnetic Storms*, AGU Geophysical Monograph 98, 253, 1997.
- Dmitriev, V., and M. Berdichevsky, The fundamental model of magnetotelluric sounding, *IEEE Proc.*, **67**, 1034, 1979.

- Engels, M., T. Korja, and BEAR Working Group, Multisheet modelling of the electrical conductivity structure in the Fennoscandian Shield, *Earth Planets Space*, **54**, 559, 2002.
- Ferris, C., Linear Network Theory, *Charles E. Merrill Books, Inc., Columbus, Ohio*, 1962.
- Feynman, J., On space weather consequences and predictions, *J. Geophys. Res.*, **105**, 10543, 2000.
- Frischknecht, F.C., Electromagnetic Physical Scale Modeling, *Electromagnetic Methods in Applied Geophysics*, **1**, Ed. M.N. Nabighian, 365, 1988.
- Fukushima, N., Generalized theorem of no ground magnetic effect of vertical currents connected with the Pedersen currents in the uniform-conducting ionosphere, *Rep. Ionos. Space Res. Jpn.*, **30**, 35, 1976.
- Gradshteyn, I.S., and I.M. Ryzhik, Table of integrals series and products, *Academic Press*, 1965.
- Gummow, R.A., GIC effects on pipeline corrosion and corrosion control systems, *J. Atmos. Sol.-Terr. Phys.*, **64**, 1755, 2002.
- Haines, G.V., Spherical cap harmonic analysis, *J. Geophys. Res.*, **90**, 2583, 1985.
- Harang, L., Maximalwerte der Erdstrom in der Nähe der Nordlichtzone während sehr intensiver erdmagnetischer Störungen, *Gerl., Beitr. Geophys.*, **57**, 310, 1941.
- Henriksen, J.F., R. Elvik, and L. Gransen, Telluric Current Corrosion on Buried Pipelines, *Proceedings of the 8th Scandinavian Corrosion Congress*, NKM 8, 167, 1978.
- Huttunen, K.E.J., H.E.J Koskinen, T.I. Pulkkinen, A. Pulkkinen, M. Palmroth, April 2000 storm: Solar wind driver and magnetospheric response, *J. Geophys. Res.*, **107**, doi: 10.1029/2002JA0099154, 2002.
- Häkkinen, L., T.I. Pulkkinen, H. Nevanlinna, R. Pirjola, and E. Tanskanen, Effects of induced currents on Dst and on magnetic variations at mid-latitude stations, *J. Geophys. Res.*, **107**, SMP 7-1 - SMP 7-8, 2002.

- Janhunen P., GUMICS-3 - A Global Ionosphere-Magnetosphere Coupling simulation with High Ionospheric Resolution, *ESA symposium Proceedings on Environment Modelling for Space-based Applications*, ESTEC, Noordwijk, NL, 233, September 2000.
- Jansen, F., R. Pirjola, and R. Favre, Space weather: Hazard to Earth?, Swiss Re Publishing, 2000.
- Jordan, E.C., Electromagnetic Waves and Radiating Systems, *New York, Prentice-Hall, Inc.*, 1950.
- Kallio, E., T.I. Pulkkinen, H.E.J. Koskinen, and A. Viljanen, Loading-unloading processes in the nightside ionosphere, *J. Geophys. Res.*, **27**, 1627, 2000.
- Kamide, Y., and W. Baumjohann, Magnetosphere-ionosphere coupling, *Physics and Chemistry in Space*, **23**, 178 p., 1993.
- Kamide, Y., Geomagnetic Storms as a Dominant Component of Space Weather: Classic Picture and Recent Issues, *Space Storms and Space Weather Hazards*, Nato Science Series, Kluwer Academic Publishers, 43, 2001.
- Kappenman, J.G., and V.D. Albertson, Bracing for Geomagnetic Storms, *IEEE Spectrum*, March 1990, 27, 1990.
- Kappenman, J.G., Geomagnetic Storms and Their Impact on Power Systems, *IEEE Power Eng. Rev.*, May 1996, 5, 1996.
- Kappenman, J.G., W.A. Radasky, J.L. Gilbert, and I.A. Erinmez, Advanced geomagnetic storm forecasting: a risk management tool for electric power system operations, *IEEE T. Plasma Sci.*, **28**, 2114, 2000.
- Keller, G., and F. Frischknecht, Electrical Methods in Geophysical Prospecting, *Pergamon Press*, 1970.
- Kisabeth, J., and G. Rostoker, Modelling of three-dimensional current systems associated with magnetospheric substorms, *Geophys. J. R. astr. Soc.*, **49**, 655, 1977.
- Klimas, A.J., J.A. Valdivia, D. Vassiliadis, D.N. Baker, M. Hesse, and J. Takalo, Self-organized criticality in the substorm phenomenon and its relation to localized reconnection in the magnetospheric plasma sheet, *J. Geophys. Res.*, **105**, 18765, 2000.

- Koen, J., Geomagnetically induced currents in the Southern African electricity transmission network, PhD thesis, *University of Cape Town*, 2002.
- Korja, T., M. Engels, A.A. Zhamaletdinov, A.A. Kovtun, N.A. Palshin, M.Yu. Smirnov, A. Tokarev, V.E. Asming, L.L. Vanyan, I.L. Vardaniants, and the BEAR Working Group, Crustal conductivity in Fennoscandia - a compilation of a database on crustal conductance in the Fennoscandian Shield, *Earth, Planets and Space*, **54**, 535, 2002.
- Koskinen, H., E. Tanskanen, R. Pirjola, A. Pulkkinen, C. Dyer, D. Rodgers, P. Cannon, J.-C. Mandeville, and D. Boscher, Space weather effects catalogue, *Finnish Meteorological Institute, Reports*, **2001:2**, 2001.
- Lahiri, B.N, and A.T. Price, Electromagnetic induction in non-uniform conductors and the determination of the conductivity of the earth from terrestrial magnetic variations, *Phil. Trans. Roy. Soc. Lond.*, **A237**, 509, 1938.
- Lam, H., D. Boteler, and L. Trichtchenko, Case studies of space weather events from their launching on the Sun to their impacts on power systems on the Earth, *Ann. Geophys.*, **20**, 1073, 2002.
- Langlois, P., L. Bolduc, and M.C. Chouteau, Probability of Occurrence of Geomagnetic Storms Based on a Study of the Distribution of the Electric field Amplitudes Measured in Abitibi, Québec, in 1993-94, *J. Geomagn. Geoelectr.*, **48**, 1033, 1996.
- Lanzerotti, L.J., and G.P. Gregori, Telluric Currents: The Natural Environment and Interactions with Man-made Systems, *The Earth's Electrical Environment*, Nat. Acad. Press, Washington, DC, 232, 1986.
- Lanzerotti, L.J., Space Weather Effects on Technologies, *Space Weather*, AGU Geophysical Monograph 125, 11, 2001.
- Lanzerotti, L., D. Thomson, and C. MacLennan, Engineering Issues in Space Weather, *Modern Radio Science 1999*, Published for the International Union of Radio Science by Oxford University Press, 1999.
- Lehtinen, M., and R. Pirjola, Currents produced in earthed conductor networks by geomagnetically-induced electric fields, *Ann. Geophys.*, **3**, 4, 479, 1985.
- Loomis, E., The Great Auroral Exhibition of August 28th to September 4th, 1859, *American Journal of Sciences and Arts*, **78**, 1859.

- Lundstedt, H., AI techniques in geomagnetic storm forecasting, *Magnetic Storms*, AGU Geophysical Monograph 98, 243, 1997.
- Mareschal, M., Modelling of natural sources of magnetospheric origin in the interpretation of regional induction studies: a review, *Surveys in Geophysics*, **8**, 261, 1986.
- Martin, B.A., Telluric Effects on a Buried Pipeline, *Corrosion*, **49**, 343, 1993.
- McNish, A., Magnetic storms, *Edison Elec. Inst. Bull.*, 361, July 1940.
- Medford, L.V., L.J. Lanzerotti, J.S. Krauss, and C.G. MacLennan, Trans-Atlantic earth potential variations during the March 1989 magnetic storms, *Geophys. Res. Lett.*, **16**, 1145, 1989.
- Mersmann, U., W. Baumjohann, F. Küppers, and K. Lange, Analysis of an eastward electrojet by means of upward continuation of ground-based magnetometer data, *J. Geophys.*, **45**, 281, 1979.
- Molinski, T., Why utilities respect geomagnetically induced currents, *J. Atmos. Sol-Terr. Phy.*, **64**, 1765, 2002.
- Mäkinen, T., Geomagnetically Induced Currents in the Finnish Power System, *Geophysical Publications, No. 32, Finnish Meteorological Institute*, 101 p., 1993.
- Ogunade, S.O., Induced Electromagnetic Field in Oil Pipelines Under Electrojet Current Sources, *Physics of the Earth and Planetary Interiors*, **43**, 307, 1986.
- Pang, K., and K. Yau, Ancient Observations Link Changes in Sun's Brightness and Earth's Climate, *EOS Transactions*, **83**, 481, October 2002.
- Pirjola, R., Electromagnetic induction in the Earth by a plane wave or by fields of line currents harmonic in time and space, *Geophysica*, **18**, 1, 1982.
- Pirjola, R., and M. Lehtinen, Currents Produced in the Finnish 400 kV Power Transmission Grid and in the Finnish Natural Gas Pipeline by Geomagnetically-Induced Electric Fields, *Ann. Geophys.*, **3**, 4, 485, 1985.
- Pirjola, R., and A. Viljanen, Complex image method for calculating electric and magnetic fields produced by an auroral electrojet of finite length, *Ann. Geophys.*, **16**, 1434, 1998.

- Pirjola, R., Geomagnetic effects on Ground-Based Technological Systems, *Review of Radio Science*, URSI, 473, 2002.
- Prescott, G.B., History, Theory and Practice of the Electric Telegraph, 4th ed., Ticknor and Fields, Boston, Massachusetts, 1866.
- Press, W.H., S.A. Teukolsky, W.T. Vetterling, and B.P. Flannery, Numerical recipes in FORTRAN: the art of scientific computing, 2nd ed., Cambridge University Press, Cambridge, 1992.
- Pulkkinen A., A. Viljanen, R. Pirjola and BEAR Working Group, Large Geomagnetically Induced Currents in the Finnish High-Voltage Power System, *Finnish Meteorological Institute, Reports*, **2000:2**, 2000.
- Pulkkinen, A., R. Pirjola, D. Boteler, A. Viljanen, and I. Yegorov, Modelling of space weather effects on pipelines, *J. Appl. Geophys.*, **48**, 233, 2001a.
- Pulkkinen, A., A. Viljanen, K. Pajunpää, and R. Pirjola, Recordings and occurrence of geomagnetically induced currents in the Finnish natural gas pipeline network, *J. Appl. Geophys.*, **48**, 219, 2001b.
- Pulkkinen, A., O. Amm, A. Viljanen, and BEAR Working Group, Ionospheric equivalent current distributions determined with the method of spherical elementary current systems, *J. Geophys. Res.*, **108**, doi: 10.1029/2001JA005085, 2003a.
- Pulkkinen, A., A. Thomson, E. Clarke, and A. McKay, April 2000 geomagnetic storm: ionospheric drivers of large geomagnetically induced currents, *Annales Geophysicae*, **21**, 709, 2003b.
- Pulkkinen, A., O. Amm, A. Viljanen, and BEAR Working Group, Separation of the geomagnetic variation field on the ground into external and internal parts using the spherical elementary current system method, *Earth, Planets and Space*, **55**, 117, 2003c.
- Robinson, R.M, and R.A. Behnke, The U.S. National Space Weather Program: A Retrospective, *Space Weather*, AGU Geophysical Monograph 125, 1, 2001.
- Root, H.G., Earth-Current Effects on Communication-Cable Power Subsystems, *IEEE Trans. Electr. Comp.*, Vol. EMC-21, 1979.
- Rostoker, G., Phenomenology and physics of magnetospheric substorms, *J. Geophys. Res.*, **101**, 12955, 1996.

- Schuster, A., The diurnal variation of terrestrial magnetism, *Phil. Trans. Roy. Soc. Lond.*, **A180**, 467, 1889.
- Siebert, M, and W. Kertz, Zur Zerlegung eines lokalen erdmagnetischen Feldes in äusseren und inneren Anteil, *Nachr. Akad. Wiss. Göttingen, Math. - Phys. Kl. Act. IIa: 87 - 112*, 1957.
- Smith, A., Coupling of External Electromagnetic Fields to Transmission Lines, *2nd ed., Umi Research Pr.*, 1987.
- Syrjäsoo, M., Auroral monitoring network: From all-sky camera system to automated image analysis, D.Sc. thesis, *Finnish Meteorological Institute, Contributions*, **32**, 2001.
- Tanskanen, E.I., A. Viljanen, T.I. Pulkkinen, R. Pirjola, L. Häkkinen, A. Pulkkinen, and O. Amm, At substorm onset, 40% of AL comes from underground, *J. Geophys. Res.*, **106**, 13119, 2001.
- Tanskanen, E., Terrestrial substorms as a part of global energy flow, PhD thesis, *Finnish Meteorological Institute, Contributions*, **36**, 2002.
- Thomson, D.J., and J.T. Weaver, The complex image approximation for induction in a multilayered Earth, *J. Geophys. Res.*, **80**, 123, 1975.
- Trichtchenko, L., and D. Boteler, Specification of geomagnetically induced electric field and currents in pipeline, *J. Geophys. Res.*, **106**, 21039, 2001.
- Tsurutani, B., and W. Gonzalez, The interplanetary causes of magnetic storms: A review, *Magnetic Storms*, AGU Geophysical Monograph 98, 77, 1997.
- Tsurutani, B., The interplanetary causes of magnetic storms, substorms and geomagnetic quiet, *Space Storms and Space Weather Hazards*, Nato Science Series, Kluwer Academic Publishers, 103, 2001.
- Untiedt, J., and W. Baumjohann, Studies of polar current systems using the IMS Scandinavian magnetometer array, *Space Sci. Rev.*, **63**, 245, 1993.
- Viljanen, A., and R. Pirjola, Statistics on Geomagnetically-induced Currents in the Finnish 400 kV Power System Based on Recordings of Geomagnetic Variations, *J. Geomag. Geoelectr.*, **41**, 411, 1989.
- Viljanen, A., K. Kauristie, and K. Pajunpää, On induction effects at EIS-CAT and IMAGE magnetometer stations, *Geophys. J. Int.*, **121**, 893, 1995.

- Viljanen, A., The relation between geomagnetic variations and their time derivatives and implications for estimation of induction risk, *J. Geophys. res.*, **24**, 631, 1997.
- Viljanen, A., Relation of geomagnetically induced currents and local geomagnetic variations, *IEEE Trans. Pow. Del.*, **13**, 1285, 1998.
- Viljanen, A., O. Amm, and R. Pirjola, Modeling geomagnetically induced currents during different ionospheric situations, *J. Geophys. Res.*, **104**, 28059, 1999.
- Viljanen, A., H. Nevanlinna, K. Pajunpää, and A. Pulkkinen, Time derivative of the horizontal geomagnetic field as an activity indicator, *Ann. Geophys.*, **19**, 1107, 2001.
- Viljanen, A., A. Pulkkinen, O. Amm, R. Pirjola, T. Korja, and BEAR Working Group, Fast computation of the geoelectric field using the method of elementary current system, Submitted to *Ann. Geophys.*, 2003.
- Wait, J., and K. Spies, On the image representation of the quasi-static fields of a line current source above the ground, *Canadian Journal of Physics*, **47**, 2731, 1969.
- Wallerius, A., Solen Gav Sverige en Strömstöt, (written in Swedish) *Ny teknik Teknisk tidskrift*, **29**, 3, 1982.
- Weaver, J.T., On the separation of Local Geomagnetic Fields into External and Internal Parts, *Zeitschrift für Geophysik*, **30**, 29, 1964.
- Weaver, J.T., Mathematical Methods for Geo-electromagnetic Induction, *Applied and engineering mathematics series*, Research Studies Press Ltd., 1994.
- Weigel, R.S., A.J. Klimas, and D. Vassiliadis, Solar-wind coupling and predictability of ground magnetic fields and their time derivatives, in press, *J. Geophys. Res.*, 2003.
- Withbroe, G.L., Living With a Star, *Space Weather*, AGU Geophysical Monograph 125, 45, 2001.



# Index

- aa\** index, 14
- adjustment distance, 45
- admittance, 45
- analogue modeling, 7
- aurora, 4
  - detection, 64
- auroral zone, 8, 54, 56
- causality, 31
- complex image method, 16, 35, 40
- complex skin depth, 37
- complex square root, 29
- conductivity, vii, 15, 25, 27, 35
  - effective, 32, 35
- convection, 55
- coronal hole, 6, 7
- coronal mass ejection, 6, 7
- corrosion, 12
- curl-free condition, 17
- current wedge, 55
- cusp, 57
- diffusion equation, 27
- direct-current, 39
- displacement current, 27
- distributed source transmission line
  - theory, 45
- divergence-free condition, 17, 20, 27
- Earth
  - homogeneous, 35, 40
  - layered, 27, 29, 35, 38
- electrojet, 50, 55
- elementary current system method,
  - 16, 38
- ESA, i, 5
- European Union, 6
- extreme events, 64
- field-aligned currents, 6, 18, 20
- Fourier method, 25
- Fourier transformation, 28, 35, 38
- Gauss-Schmidt method, 25
- geoelectric field
  - modeling, 28, 35
  - properties, 26, 49
- geomagnetic storm, *see* magnetic storm
- geomagnetically induced currents,
  - 10
  - economic impact, 10
  - effects
    - communication cables, 11
    - pipelines, 12
    - power systems, 10
    - railways, 12
    - telegraph, 4, 6, 10
  - forecast, 63
  - modeling
    - continuously grounded systems, 45
    - discretely grounded systems, 39

- reported occasions, 14
- Green's function, 18
- half-cycle saturation, 10
- impedance, 29, 30, 35, 36, 40, 45
- ionospheric currents, *see* ionospheric equivalent currents
- ionospheric equivalent currents
  - classification, 64
  - derivation, 16
  - properties, 54
- $K$  index, 52
- Kirchhoff's law, 43
- least squares, 22, 26
- linearly varying field, 33
- magnetic field separation, 23, 24, 63
- magnetic pulsations, 56
- magnetic storm, 6, 8, 56
- magnetohydrodynamic modeling, 63
- magnetosphere, 3, 8, 56
- magnetotelluric method, 34, 63
- Maxwell's equations, 26
- neural networks, 63
- NOAA, 5
- Ohm's law, 26
- omega band, 56
- pattern recognition, 64
- permeability, vii, 26
- permittivity, vii
- plane wave method, 34, 52
- power law, 64
- quasi-static field, 27, 31
- reconnection, 8
- scaling factor, 21, 22, 25, 39
- sea-continent boundary, 63
- self organized criticality, 57, 64
- singular value decomposition, 22, 26
- skin depth, 51
- solar wind, 3, 7
- space environment center, 5
- space weather
  - definition, 4
  - economic impact, i
  - effects, 4
  - physics, 7
- spatial method, 25
- spectral impedance, *see* impedance
- spherical cap harmonic analysis, 16, 25
- spherical elementary current system method, *see* elementary current system method
- spherical harmonic method, 16
- substorm, 8, 55, 56, 64
- sudden commencement, 56
- Sun, 3, 7
- Thevenin theorem, 46
- time derivative of the magnetic field, 35, 50
- US Air Force, 5